Mon. Not. R. astr. Soc. (1991) **248**, 233–255

Optical and X-ray observations of AO Piscium and the origin of the spin pulse in intermediate polars

Coel Hellier, Mark Cropper and Keith O. Mason

Mullard Space Science Laboratory, University College London, Holmbury St. Mary, Dorking, Surrey RH5 6NT

Accepted 1990 July 23. Received 1990 July 20; in original form 1990 April 4

SUMMARY

Observations of AO Psc are presented which suggest that it has a magnetic field much weaker than the AM Her stars, that it possesses an accretion disc extending inwards to ~ 8 white-dwarf radii and outwards to fill the Roche lobe, and that it accretes on to narrow arcs around the magnetic poles of the white dwarf with areas $\lesssim 0.01$ of the white-dwarf surface. We exclude the alternative of an intermediate polar having a field similar to the AM Her stars, not possessing a disc, and accreting primarily through ballistic 'blobs' which strike the white dwarf over ~ 0.5 of its surface.

It is argued that the spin-modulated components of the X-ray, optical-continuum and line emission originate in magnetically controlled 'accretion curtains' above the white dwarf's magnetic poles. The modulations are all caused by the variation in our view of the optically thick accretion curtain with spin phase. When the upper pole points away from the observer, we see maximum area of the accretion curtain and hence maximum flux; the material is flowing on to the pole from the far side of the disc, producing blueshifted emission lines. Occultation due to the upper pole disappearing over the limb does not contribute significantly to the modulation of the X-ray light curve, implying that any disappearance is compensated for by the simultaneous appearance of the lower pole. Hence, we must see similar X-ray fluxes from both poles.

Intensity dips in both the X-ray light curve and the optical emission lines are caused by material thrown out of the orbital plane, perhaps by the impact of the accretion stream with the disc, in a manner analogous to the dipping activity of many low-mass X-ray binaries. This implies a moderately high inclination of ~ 60°.

The different amplitudes of the optical spin-pulses from one star to another can be explained by different locations of the emission region within the accretion curtain, coupled with the effect of inclination. The spin-pulse amplitude is greatest when the system is viewed edge-on.

1 INTRODUCTION

AO Psc (H2252 − 035) is a member of the intermediate polar sub-class of cataclysmic binary in which the accretion flow from the red dwarf encounters a magnetic white dwarf. The magnetically channelled accretion results in the signature of intermediate polars: X-ray emission pulsed at the white dwarf's spin period. After White & Marshall (1981) had discovered AO Psc's 805 s spin period from X-ray light curves, an optical modulation at this frequency was also found (Warner, O'Donoghue & Fairall 1981). However, the optical light curves are normally dominated by variations at two previously discovered periods, 3.59 hr and 859 s (Patterson & Price 1981). As the 859 s period is the beat period between the other two, the accepted model identifies the 3.59 hr modulation with the orbital cycle and explains the 859 s pulse as the result of reprocessing of spin-pulsed X-rays by material fixed in the binary frame.

Spectroscopic observations of AO Psc detect strong hydrogen and helium emission lines which show radial velocity and flux modulations with the orbital, spin and beat periods (Patterson & Price 1981; Penning 1985; Wickramasinghe, Stobie & Bessell 1982). *EXOSAT* observations (Pietsch *et al.* 1987) confirmed the dominant spin modulation of the X-ray light curve and also detected shallow dips lasting about half an hour, recurring with the orbital cycle.

In this paper we present three nights of time-resolved spectroscopy obtained to analyse the emission-line variations with AO Psc's three periods. We also analyse the *EXOSAT* observations to enable a comparison with the optical data in modelling this star. We compare our findings with those from other intermediate polars and discuss the implications for the class as a whole.

2 OPTICAL SPECTROSCOPY

The observations were made at the South African Astronomical Observatory using the 1.9-m telescope, Image Tube Spectrograph and the Reticon Photon Counting System. We obtained a series of spectra, each of 1 min integration, spanning 5 hr on each of the nights 1988 August 4, 6 and 8. In total, 825 spectra were obtained. The wavelength coverage was from 4200–5000 Å at a resolution of 1.3 Å. We made regular exposures of a Cu/Ar arc to determine the wavelength calibration and we observed standard stars for flux calibration.

The phase averaged spectrum of AO Psc is shown in Fig. 1. This has been notch filtered at the four pixel frequency to remove a modulation caused by the RPCS detector. The spectrum shows the Balmer lines Hβ and Hγ, He II λ4686, He I λ4471, the C III/N III λ4640 blend and evidence for He I 4713, 4921, 5015 and O II 4416.

2.1 Continuum variations

The recorded count rate through the narrow spectroscopic slit is affected by variations in seeing and atmospheric dispersion and by guiding errors. Nevertheless, the count rate allows a direct determination of the phasing of the 14-min photometric variations. In analysing the pulse times we have restricted the data to one orbital cycle on each night in order to minimize mutual distortion by the spin and beat periods. The count rates from the first and third nights show a prominent beat-period (859 s) variation with an amplitude of 12 ± 1 and 8 ± 1 per cent respectively. In both cases the modulation is phased such that maximum light occurs at HJD 2447378.3899 ± 0.0007 (± 0.07 cycles). This is 0.1 cycles earlier than expected from extrapolating the quadratic ephemeris of Kaluzny & Semeniuk (1988), although the discrepancy is within the quoted errors. The count rate from the second night showed a much reduced beat-period variation (amplitude 2.0 ± 0.5 per cent) which allowed the modulation at the spin (805 s) period to dominate (amplitude 4.4 ± 0.6 per cent). The spin modulation has maximum light at HJD 2447378.3887 ± 0.0009 (± 0.1 cycles) which is 0.2 cycles earlier than Kaluzny & Semeniuk's quadratic spin ephemeris, although again this is within the errors. In analysing the spin and beat periods in our data we have used the phasings determined from the count rate.

The Fourier transform of the count rate from all three nights is shown in the top right panel of Fig. 2. Since observational uncertainties dominate at long periods, the transform was calculated after fitting a low-order polynomial, thus suppressing the power below 0.1 mHz. The window pattern is illustrated in Fig. 2 by transforms of sinusoidal tracers at the orbital and spin frequencies, sampled as the data.

The count rate stability is not reliable over several hours (due primarily to variations in seeing) so we are unable to reliably determine the orbital phasing, although it is consistent with the predictions of Kaluzny & Semeniuk's linear orbital ephemeris which has an extrapolated error of 0.07 cycles. Thus we have used this ephemeris for orbital analysis. We have, however, used a different phase convention. Previous authors have placed orbital phase zero at maximum light; we adopt orbital phase zero at minimum light (0.5 different) as more likely to represent inferior conjunction of the secon-

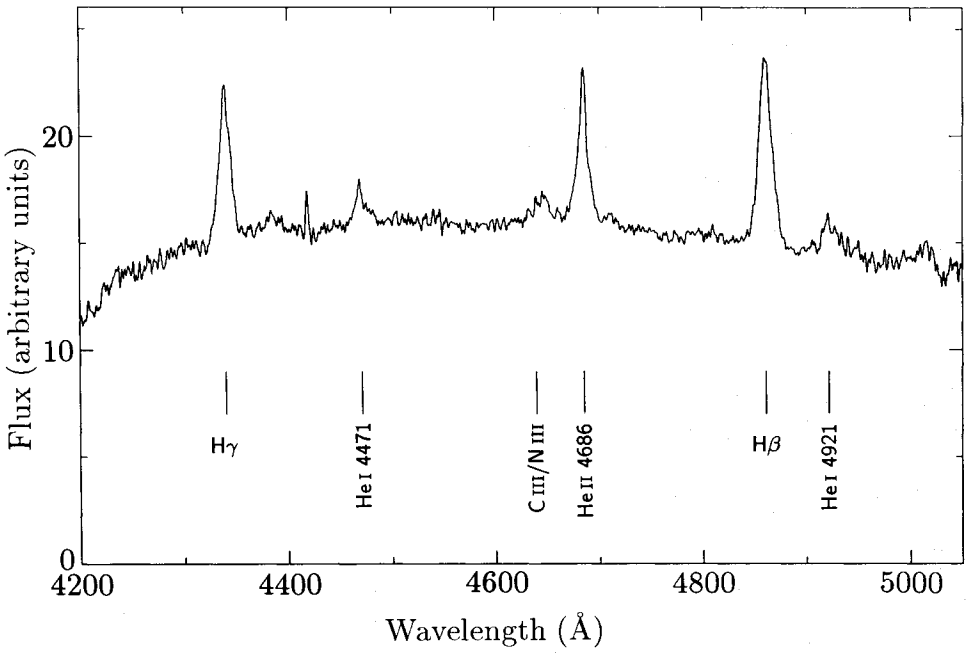

Figure 1. The phase-averaged spectrum of AO Psc.

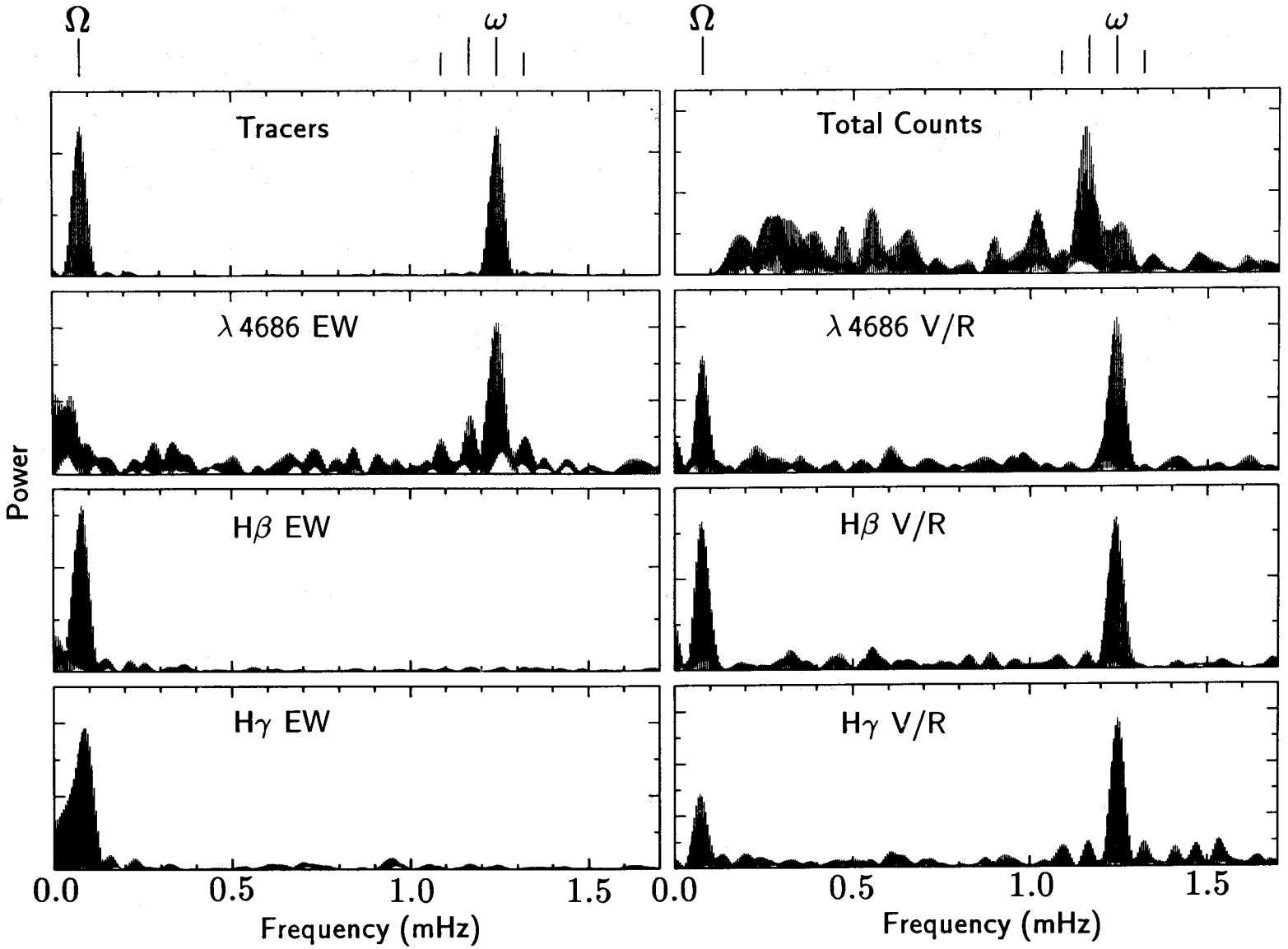

Figure 2. Fourier transforms of the equivalent widths and V/R ratios of the emission lines in AO Psc. The window pattern is illustrated by the transform of sinusoidal tracers at the orbital and spin periods, sampled as the data (top left). Top right shows the transform of the total counts in each spectrum; low-frequency noise has been suppressed. The tick marks on top indicate the orbital (Ω), spin (ω), and orbital sideband frequencies. Note that though the dominant count-rate variation occurs with the beat period, the emission lines vary with the spin period.

dary, which is usually adopted as phase zero when known. With the above phasings, the spin and beat periods are in phase at orbital phase zero (minimum). This is the same as has been found by previous authors (van Amerongen *et al.* 1985, and references therein) which confirms the correctness of our phasings.

2.2 Periodic variation of the emission lines

We have analysed variations in the emission lines in each spectrum of AO Psc using the orthogonal measures, the equivalent width and the V/R ratio. The latter is the ratio of the equivalent widths on each side of the rest wavelength. The Fourier transforms of these quantities are shown in Fig. 2. Note that although the dominant continuum variation is at the beat period (top right), the emission lines vary predominantly with the spin period. The Balmer lines show no equivalent-width variation with either spin or beat periods (the lines fluxes will therefore follow the continuum with a beat-period modulation). He II λ4686 shows a large spin-period variation in equivalent width together with a smaller beat-period variation and also power at the $\omega - 2\Omega$ and $\omega + \Omega$ sidebands (where Ω is the orbital frequency and ω the spin frequency). All lines show a prominent V/R spin-period modulation with only slight evidence for sidebands, strongest in the Hγ line. With the orbital period, all lines vary in both equivalent width and V/R ratio.

2.3 The orbital cycle

The orbital-cycle variations of equivalent width and V/R ratio are shown in Fig. 3, while Plate 1 shows a grey-scale plot of the line profiles folded on the orbital period. The essential features of the lines are as follows. A substantial *S*-wave feature is present in all lines (most obvious in He II λ4686) and extends as far into the line wings as they can be traced. This variation dominates over the orbital velocity of the white dwarf and causes a V/R variation phased with maximum redshift near phase 0.25. The equivalent widths of the Balmer and He I λ4471 lines show a large drop between phases 0.0 and 0.3, which is also present at a lower level in He II λ4686. From Plate 1, it is seen that this is due to a pronounced dip in the centre of the line profiles with a full width of ~ 400 km s^{-1}. During these phases the centre of the He I λ4471 line goes into absorption (i.e. lies below the continuum). A further component seen in He II λ4686 is a narrow emission feature dominating the line core and showing little or no velocity modulation. Fig. 4 shows the individual phase-resolved line profiles over the orbital cycle. Since the emission lines are dominated by the *S*-waves and the dips, we are unable to measure the orbital velocity of the primary from the emission lines.

2.3.1 The He II λ4686 line

The He II λ4686 line shows the best defined *S*-wave and narrow component. We have attempted to parameterize these components by a multi-Gaussian fit to the phase-resolved profiles. To minimize distortions due to spin-cycle variations we used 16 phase bins over the orbital cycle giving bins almost exactly 1 spin cycle long. We found that three Gaussians were required to describe the line adequately. A

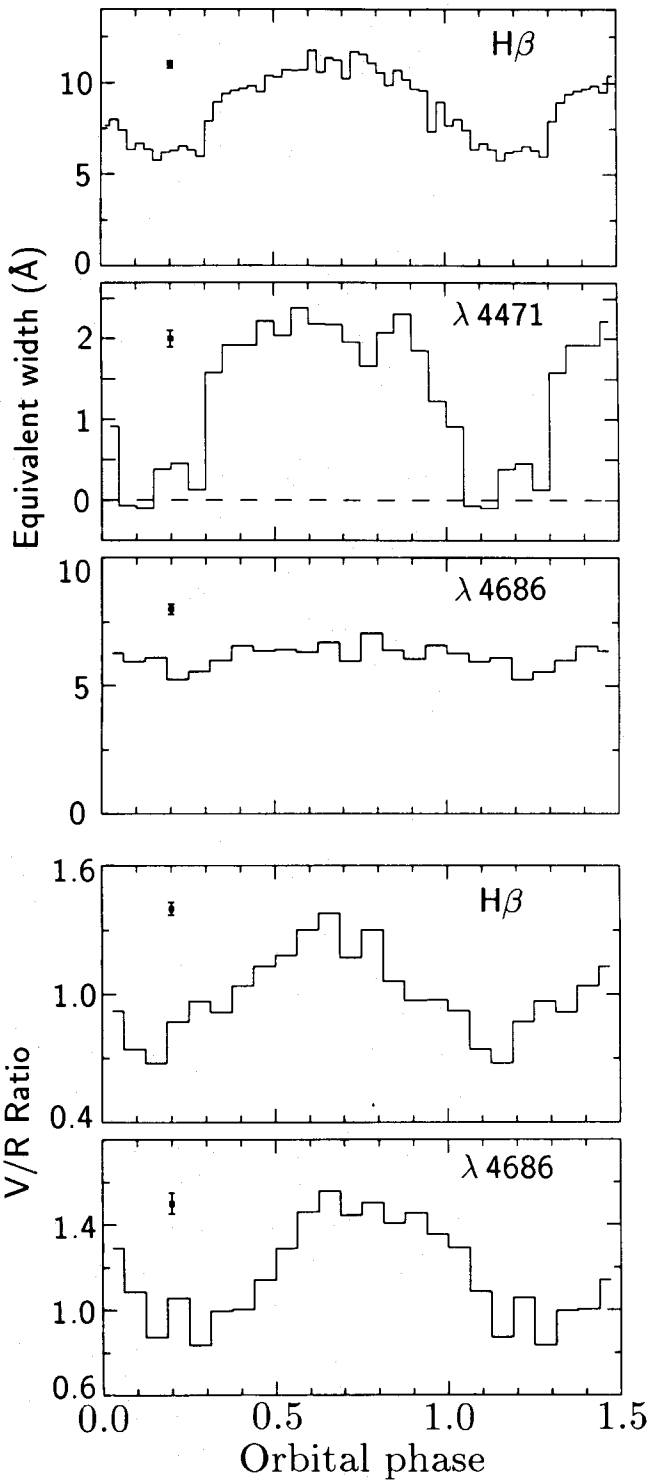

Figure 3. Equivalent widths and V/R ratios folded on the orbital cycle. We have used Kaluzny & Semeniuk's (1988) ephemeris.

Gaussian with FWHM near 2 Å modelled the narrow component, another with FWHM near 3.5 Å traced the *S*-wave while a further low-level Gaussian with FWHM around 8 Å was required to represent the base of the line. No parameters were constrained during the fitting. A typical decomposition into three Gaussians is illustrated in the inset to Fig. 5. A

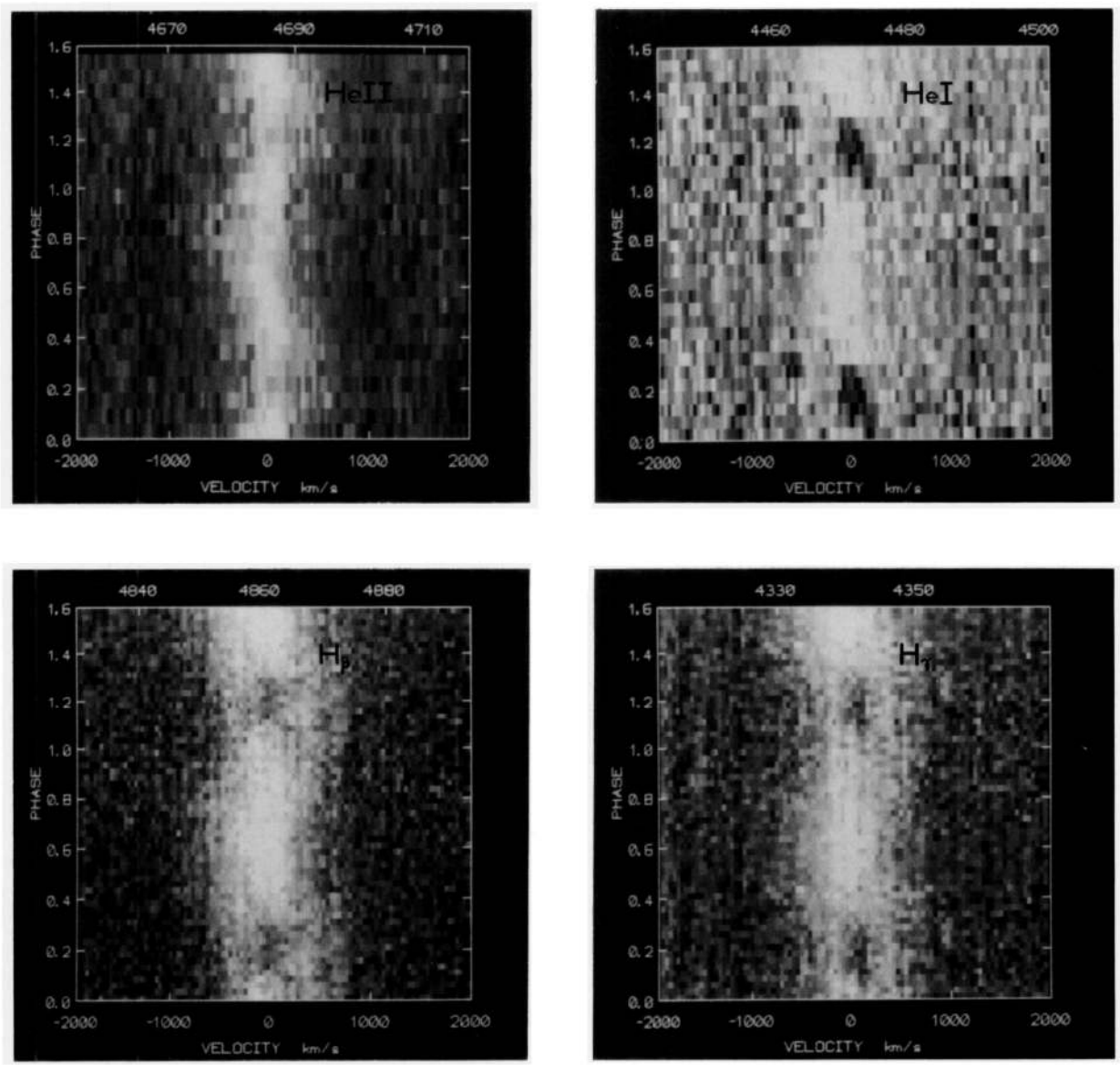

Orbital Cycle

Plate 1. Grey-scale representations of the line profiles of AO Psc folded on the orbital period. The line intensities have been normalized to the continuum. The phasing accords to Kaluzny & Semeniuk's (1988) ephemeris. Note the 'dips' in the line near phase zero, corresponding to similar dips in the X-ray light curves. The line motion is dominated by an *S*-wave caused by the impact of the mass-transfer stream with the disc, rather than by the orbital velocity of the white dwarf.

[*facing page* 236]

1991MNRAS.248..233H

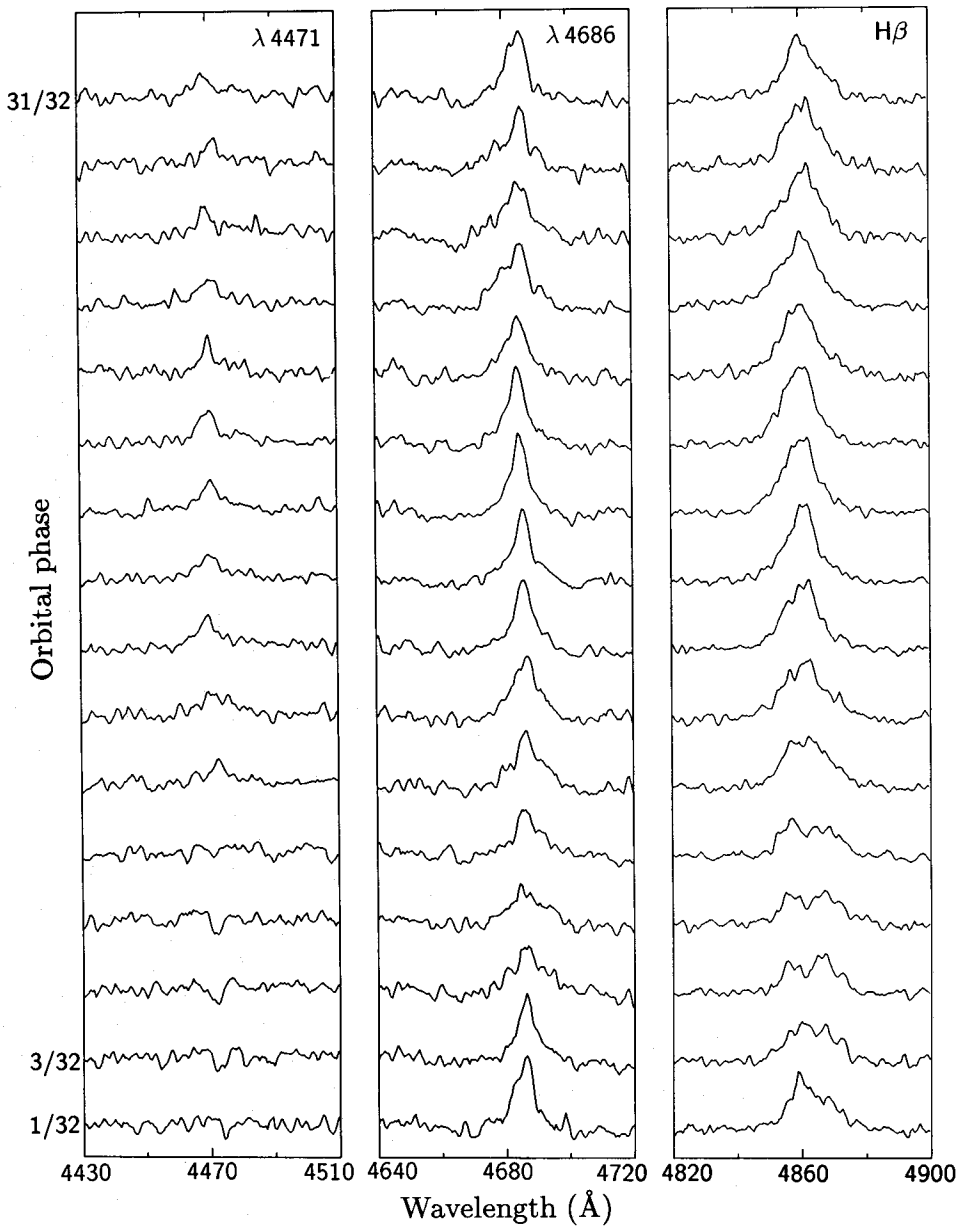

Figure 4. Phase-binned line profiles of the He I λ4471, He II λ4686 and Hβ lines over the orbital cycle. All data have been normalized to the continuum level.

sinusoid fit to velocities of the *S*-wave component then yielded a semi-amplitude of 400 ± 30 km s^{-1} phased with maximum redshift at 0.28 ± 0.03. The γ velocity was 20 ± 40 km s^{-1} and the mean FWHM of the fitted Gaussian was 240 ± 30 km s^{-1}. The narrow component showed no significant velocity variation with a 90 per cent confidence upper limit of 80 km s^{-1}. The mean FWHM of the feature was 130 ± 8 km s^{-1}. This, though, is not far above the instrumental broadening of 80 km s^{-1} and so is unreliable. The broad base component had a mean FWHM of 530 ± 30 km s^{-1} but also showed no significant velocity modulation. This component was the least well defined and the 90 per cent confidence upper limit on motion is 150 km s^{-1}. Fig. 5 shows the radial-velocity curves of the three components and the best-fit sinusoids.

2.3.2 *Comparison with previous reports*

Wickramasinghe *et al.* (1982) reported features of the orbital-period line behaviour which agree with our data. They detected a similarly phased *S*-wave, with maximum redshift 0.2 after orbital minimum, while also at this phase the Balmer lines showed double peaks, the equivalent widths dropped and the He I λ4471 line disappeared.

Wickramasinghe *et al.* investigated the Hβ line by measuring the radial velocities of three components; the base up to 20 per cent of the peak above the continuum, the separate red and blue peaks where they could be distinguished, and the main peak where separate red and blue peaks could not be distinguished. From our data, however, it is clear that the appearance of two peaks is due to absorption in the line

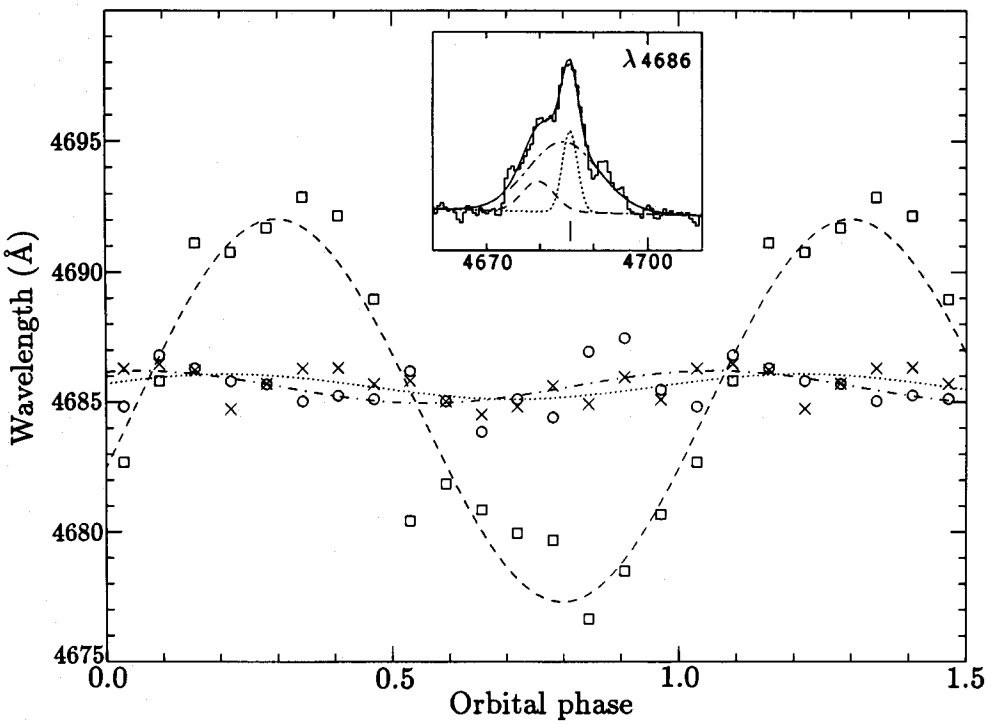

Figure 5. The radial velocities derived from a three-Gaussian decomposition of the orbitally resolved line profiles, together with the best-fit sinusoids. The inset shows a typical decomposition illustrating the three components: a broad stationary base, a central narrow stationary component, and a medium-width *S*-wave (*cf.* Plate 1 and Fig. 4).

centre rather than reflecting the velocity of the emitting material. Wickramasinghe *et al.* noted this possibility but went on to use their radial-velocity measurements to estimate the orbital velocity of the primary (60 km s^{-1}) and hence the inclination (~ 30°), results which are therefore doubtful. The parameters they found for the base *S*-wave component in the Hβ line are similar to those we find in He II λ4686. They find maximum redshift at phase 0.2 with an amplitude of 350 km s^{-1}. As the *S*-wave is a larger fraction of the line in He II λ4686, and as this line does not show the absorption dip, the He II λ4686 values for the *S*-wave are likely to be the most reliable.

2.4 The spin and beat cycles

As seen from the Fourier transforms (Fig. 2), all lines show a prominent radial-velocity motion with the spin cycle. There is no spin-cycle variation in the equivalent widths of the Balmer lines, but there is in the He II λ4686 line. The variations in these quantities are shown in Fig. 6 and the line profiles are shown in grey-scale form in Plate 2. The *V*/*R* variation is caused by a broad base in the emission lines varying in velocity with the spin cycle (easily seen in He II λ4686 in Plate 2). We refer to this feature as a 'spin-wave' by analogy with the orbital cycle *S*-waves which have a similar appearance in phase-resolved spectra. In the Balmer lines the spin-wave is superimposed on a broad stationary component while in He II λ4686 it is accompanied by a narrower stationary component.

Although the dominant photometric variation occurs with the beat ($\omega - \Omega$) period, there is little variation in the emission-line radial velocities or equivalent widths (the latter implies that the line fluxes are largely modulated as the continuum). The He II λ4686 equivalent width shows a beat-period variation which is illustrated in Fig. 6 and Plate 2. The line variation is confined to the centre of the line (Plate 2) implying that the reprocessing occurs in the low velocity outer regions of the binary system. The equivalent width is greatest at phase 1.0 indicating that the line flux is modulated to a greater extent than the continuum.

The He II λ4686 line also varies with the $\omega - 2\Omega$ and $\omega + \Omega$ sidebands (Fig. 2). This is similar to the findings of Hellier, Mason & Cropper (1990) for the intermediate polar FO Aqr where the He II λ4686 line varied at all four spin-related frequencies predicted by Warner (1986), while the Balmer lines showed little variation other than at the spin frequency itself.

2.4.1 *The He II λ4686 line over the spin cycle*

Fig. 7 shows the spin-resolved He II λ4686 line profiles which are seen in grey-scale form in Plate 2. We have decomposed the line using two Gaussians; one with FWHM near 2 Å to model the narrow component and the other with FWHM near 7 Å to model the spin-wave. No parameters were constrained while fitting the phase-binned profiles. This method gave a good description of the line. However, velocities derived in this way are of course dependent on the decomposition being physically sensible. In particular, the orbital *S*-wave will be smeared into an average profile which is not taken into account in the two Gaussian decomposition. When a further Gaussian was added, though, the decomposition was no longer stable or unique.

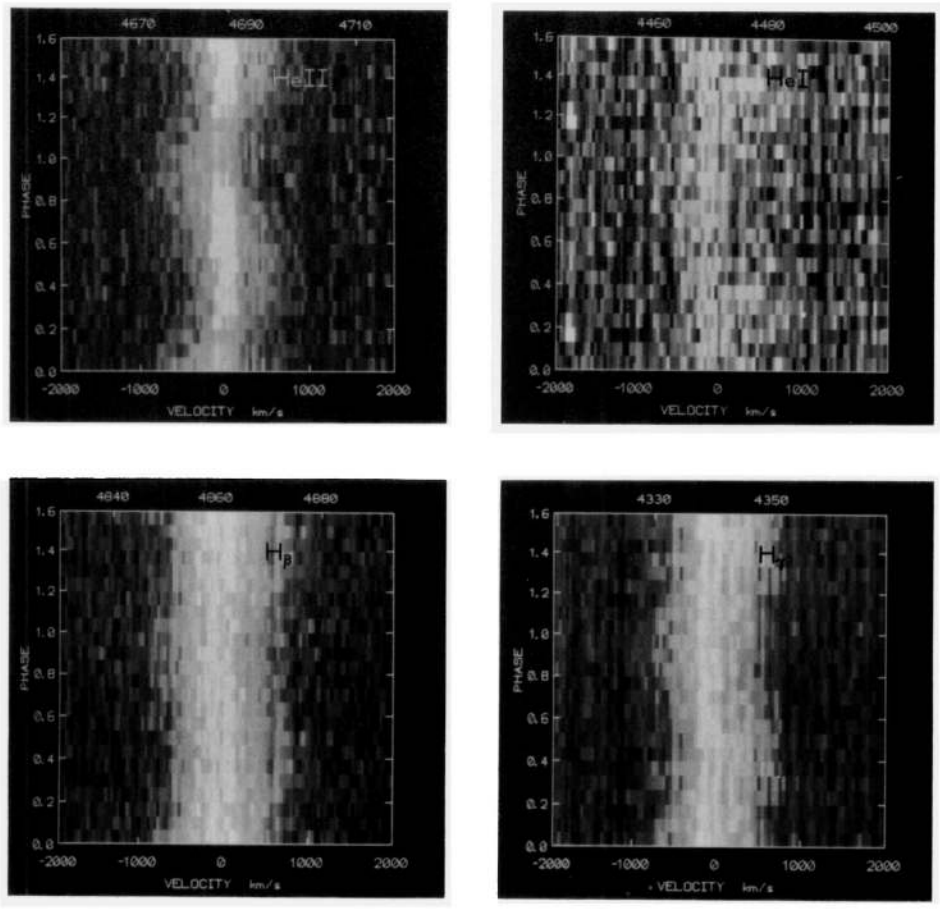

Spin Cycle

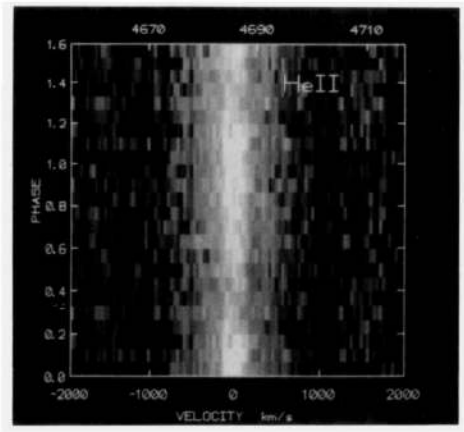

Beat Cycle

Plate 2. Grey-scale representations of the line profiles of AO Psc folded on the spin and beat periods, with phasings determined from the observed count rate. Note the broad 'spin-wave', most easily seen in He II λ4686, phased with maximum blueshift at spin maximum (phase 1).

[*facing page* 238]

1991MNRAS.248..233H

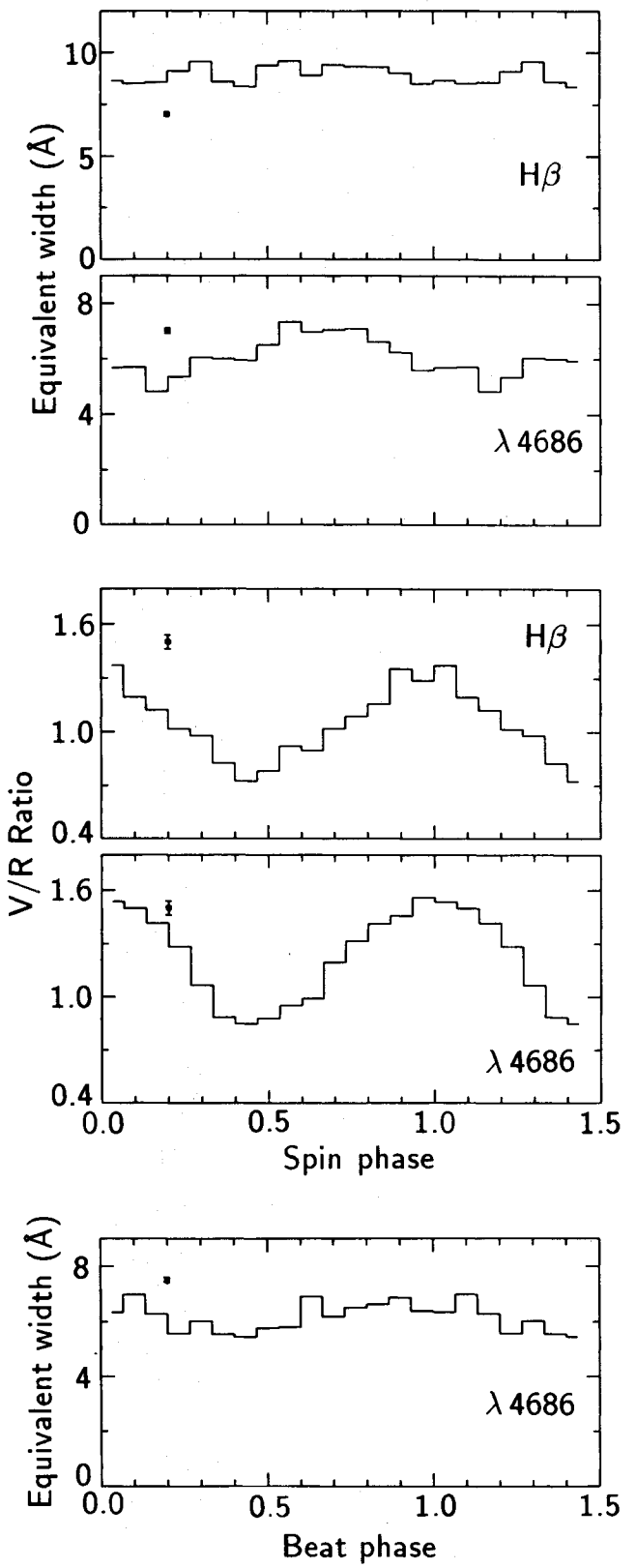

Figure 6. Equivalent widths and V/R ratios folded on the spin cycle (upper) and beat cycle (lower). The spin and beat phases were determined from the spectroscopic count rate (see text).

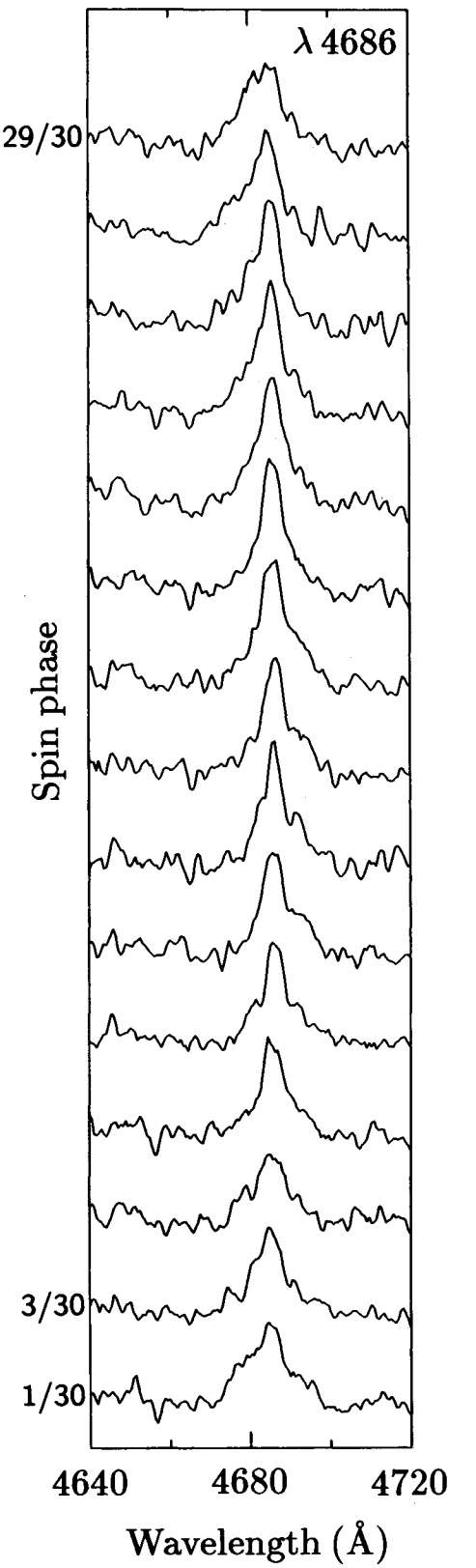

Figure 7. Phase-binned profiles of the He II λ4686 line over the spin cycle. Each profile will contain the phase-averaged variations on the other periods. The data are normalized to the continuum level.

With the two Gaussian decomposition the spin-wave has a semi-amplitude of 260 ± 30 km s^{-1} phased with maximum blueshift at phase 0.95 ± 0.03 (phase 1.0 is maximum light). The FWHM was measured as 450 ± 50 km s^{-1} and the γ velocity as -20 ± 15 km s^{-1}. The narrow component showed no detectable motion with a 90 per cent confidence limit of 70 km s^{-1}. Its mean FWHM was 125 ± 10 km s^{-1}, and its mean (γ) velocity -5 ± 12 km s^{-1}. Fig. 8 shows the velocity data and the best-fit sinusoids, together with a sample decomposition of the line profile into two Gaussians.

We have also used the two-component decomposition to investigate the equivalent-width changes in the He II λ4686 line. Fig. 9 shows the measured equivalent widths of the separate components. It is clear that both components vary;

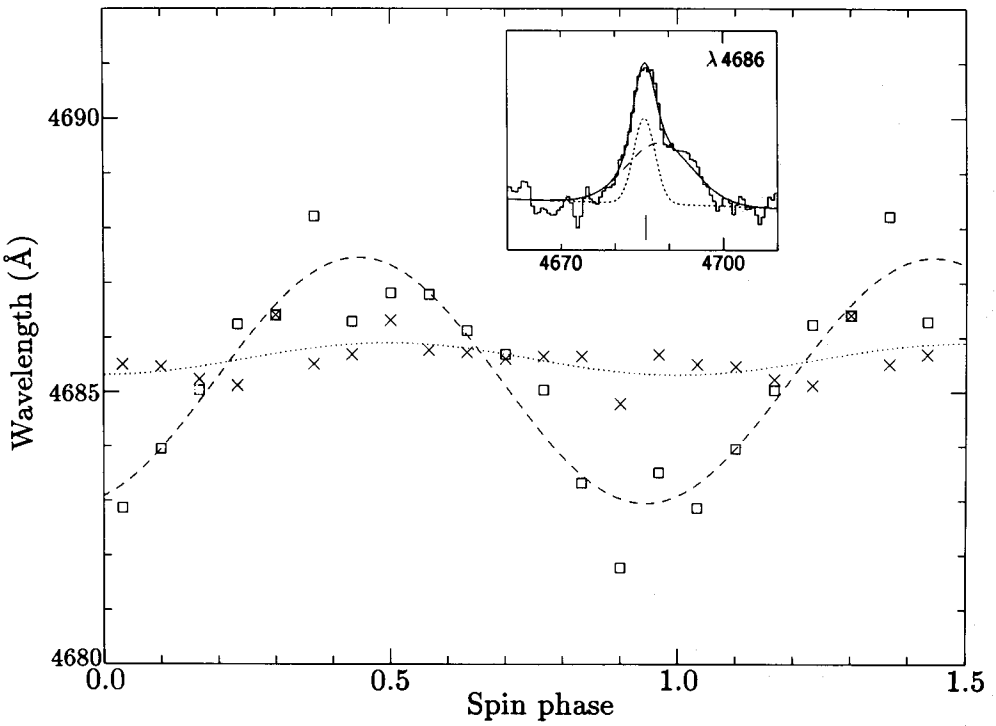

Figure 8. The radial velocities derived from a two-Gaussian decomposition of the spin-resolved line profiles, together with the best-fit sinusoids. The inset shows a typical decomposition illustrating the two components: a narrow stationary component and a broad base 'spin-wave' (*cf.* Plate 2 and Fig. 7).

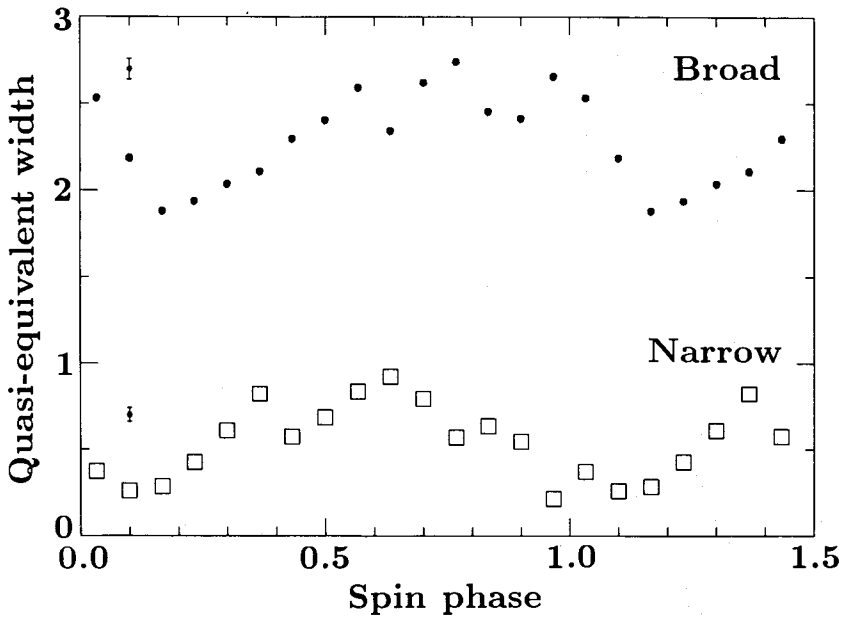

Figure 9. Equivalent widths of the narrow and broad components of the He II λ4686 line as a function of spin phase. We used a two-Gaussian decomposition as described in the text.

the narrow component is much reduced around phase 0.1 and the broad component also shows a minimum centred slightly later around phase 0.2. The variation in the narrow component is easily seen directly in the line profiles (Plate 2 and Fig. 7). The change in equivalent width is a factor of ~3 over the spin cycle and so cannot be attributed purely to the spin-cycle continuum variation which is only ~4 per cent.

2.4.2 *Comparison with previous reports*

Wickramasinghe *et al.* (1982) reported that the equivalent width of He II λ4686 was pulsed by 25 per cent with the beat period but did not vary with the spin period. They found no variation of the Balmer line equivalent widths with either period. Our findings agree in the case of the Balmer lines. We also find a He II λ4686 line beat-period variation with an amplitude and phasing similar to theirs. However, in our data there is a larger spin-period equivalent width variation in this line with a full amplitude of ~35 per cent compared to their upper limit of 15 per cent. Additionally, they found an upper limit of 50 km s^{-1} semi-amplitude on motion of both the base and peak components of the He II λ4686 line, while in our data the base component has a semi-amplitude of 260 ± 30 km s^{-1}. These discrepancies suggest that the He II λ 4686 line is substantially different at different epochs.

Radial-velocity motion of the emission lines was found by Penning (1985) who reported it to be with the spin period rather than the beat period. Hutchings & Cote (1986) also obtained phase-resolved spectroscopy of AO Psc, with an integration time of 1/4 of the beat period. With such data they were unable to distinguish effects on the beat and spin periods and so although they found both radial-velocity and equivalent-width variations it is unclear how to interpret them.

Other observations by Warner *et al.* (1981) and Clarke, Mason & Bowyer (1983) did not reveal line changes correlated with the spin or beat periods; however, this is probably explainable by the limitations of their data sets together with the substantial flickering behaviour exhibited by AO Psc.

3 *EXOSAT* OBSERVATIONS

The *EXOSAT* satellite (White & Peacock 1989) observed AO Psc on four occasions. These were, 1983 days 257 and 260, and 1985 days 296 and 299, each time for about 8 hr. Some aspects of the 1983 observations have previously been reported by Pietsch *et al.* (1985, 1987).

The X-ray light curves of AO Psc are shown in Fig. 10. Like most intermediate polar X-ray light curves, they are dominated by a nearly sinusoidal spin-period variation. In addition, periodic dips recur with the orbital cycle, during which the mean count rate drops and the spin-modulation amplitude is reduced proportionately.

3.1 The orbital-cycle dips

To investigate the orbital dips, the lower panels in each section of Fig. 10 show the *EXOSAT* light curves at a time resolution of one spin cycle, so smearing out spin-cycle effects. We also show the hardness ratio (the 4.5–8.5 keV/1.5–4.5 keV count rate) at the same resolution. The figures also give the orbital phase according to the ephemeris used for our optical data; this was derived from optical observations which span the X-ray observations in time (Section 2.1). The 1983 data show prominent dips lasting for ~50 min around optical-photometric orbital minimum (phase zero). Note the first 1983 observation where one dip is accompanied by a rise in the hardness ratio, suggestive of photoelectric absorption, while the preceding dip produces no significant change in hardness ratio. In the 1985 observations, dips again occur at orbital minimum but are much less pronounced and only marginally significant. In these dips there is marginal evidence of an increase in hardness ratio.

In the second 1983 observation, a swap of the ME-array halves occurred during the only dip recorded, while there are also marked background variations during and out of the dips. Therefore, as the 1985 dips are insufficiently deep to analyse spectral changes, we report a detailed analysis of the first 1983 observation only.

In the first 1983 observation, the on-source ME-array half was swapped midway through the observation so that approximately one orbital cycle (and one of the two dips) was recorded in each half. To ensure that we only study spectral changes related to the orbital cycle, we have accumulated spectra from portions of the light curve covering an integral number of spin cycles. A length of 10 spin cycles was taken from non-dip regions for each of the array halves. Similarly, we extracted a length of three spin cycles from each of the dips.

The non-dip spectra from each half are well fitted by a single power law with index -0.8 ± 0.1 together with an absorbing column of 6×10^{20} H atom cm^{-2}; this gave $\chi^2_\nu = 1.07$ and 1.15 ($\nu = 32$) for the data from the two detector halves. Adding an iron line at 6.7 keV did not significantly improve the fit. As these spectra are summed over the substantial changes associated with the spin cycle (see below), we adopt a power-law fit as the simplest convenient representation rather than for physical interpretation. The data from the dips have lower statistical quality due to the lower dip count rate and the shorter length of the data. They are also well fit by a single power law; however, the index is less well constrained with adequate fits obtainable in the range -0.5 to -1.3. Under the assumption that the dips are caused by viewing an unchanged central X-ray source through a cloud of material (discussed later in Section 4.1) the power-law index should be unchanged. Thus, we have modelled the dip spectra using an index fixed at -0.8 (giving best $\chi^2_\nu = 0.96$ and 0.97 for the two dips). The remaining parameters are the normalization and the absorbing column; the spectral fit contours in these parameters are plotted in Fig. 11. At lower right are the non-dip spectra from the two halves which produce similar results. The two dips, though, behave differently, as suggested by their different hardness ratios. The second dip requires a two orders of magnitude increase in absorbing column (to 5×10^{22} H atom cm^{-2}) together with a 20 per cent reduction in normalization. The first dip is well modelled with only a marginal increase in column (to 10^{22} H atom cm^{-2}), but needs a 40 per cent reduction in normalization.

The photo-ionization state of the material is characterized by the parameter, $\xi = L_x/nr^2$, where n is the number density of material at a distance r from a source of luminosity L_x. Writing n as $N_H/\varepsilon r$, where ε (< 1) is the radial extent of the material as a fraction of r, we have $\xi = \varepsilon L_x/N_H r$. Taking

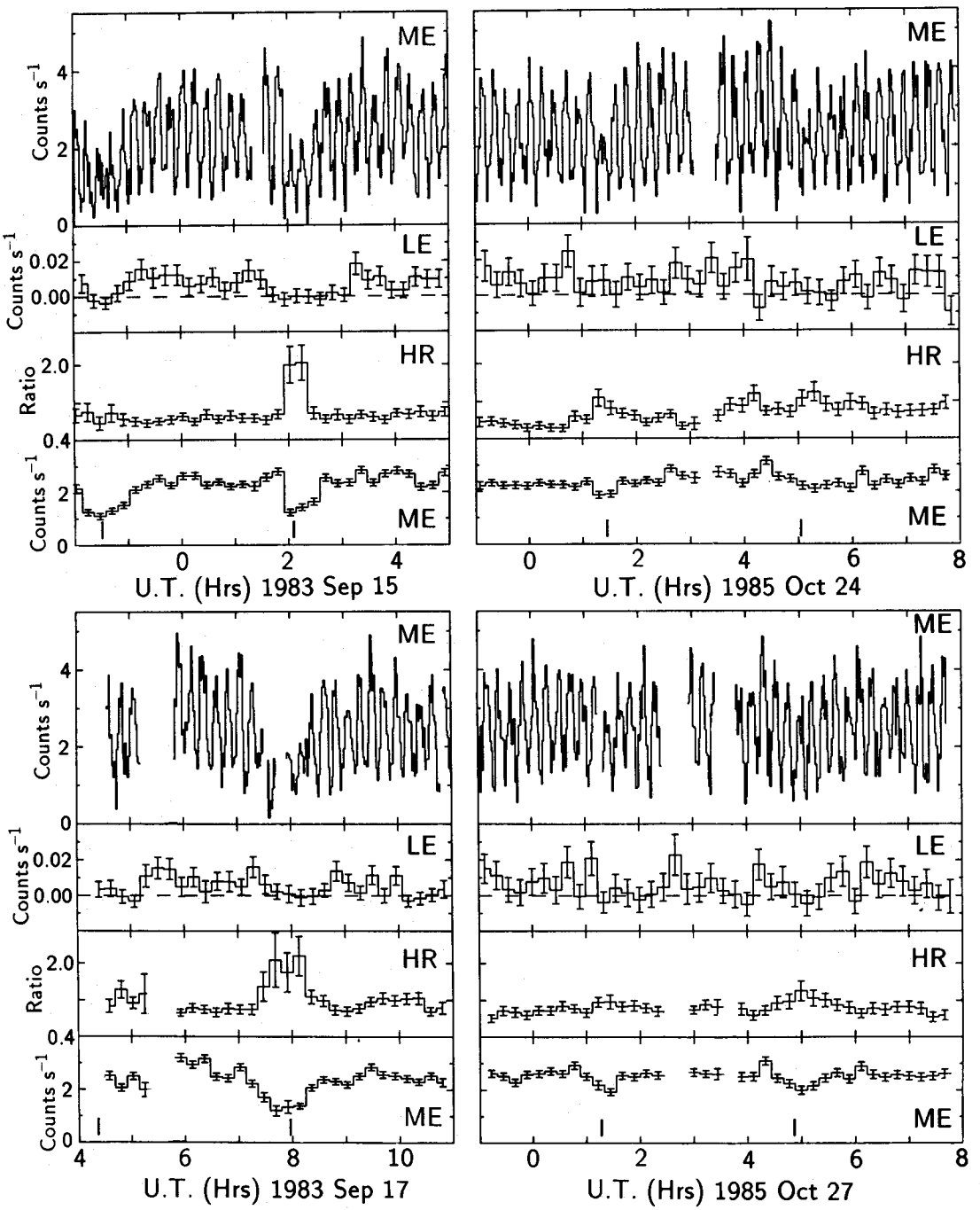

Figure 10. *EXOSAT* light curves from the four observations of AO Psc. The panels in each section show, from the top, the ME (1.5–8.5 keV) data at 80-s resolution, then the LE (0.2–2 keV) data, the ME hardness ratio (4.5–8.5/1.5–4.5 keV) and the ME data again, all at 1 spin cycle (805-s) resolution. Tick marks near the time axis give times of orbital minimum according to Kaluzny & Semeniuk's (1988) ephemeris.

$L_x = 10^{33}$ erg s^{-1}, $\varepsilon = 0.1$, $r = 5 \times 10^{10}$ cm (for the edge of the disc; see Section 4.1) and $N_H = 5 \times 10^{22}$, gives $\xi = 0.04$ which is three orders of magnitude too low for significant ionization of hydrogen and helium (Hatchett, Buff & McCray 1976). This agrees with the results from the second dip, which was modelled purely by photoelectric absorption.

The energy independence of the first dip suggests, however, that electron scattering rather than photoelectric absorption is responsible. We cannot, though, attribute the required free electrons to photo-ionization. A 40 per cent reduction in flux due to electron scattering requires a column of 1×10^{24} electrons cm^{-2}, or $\sim 1 \times 10^{24}$ H cm^{-2} with $\xi \sim 50$. For photo-ionization, taking ε at its upper limit of 1, this requires $r \sim 1 \times 10^7$ cm, which is clearly unphysical, being 1/50th of a white-dwarf radius. We must conclude, therefore, that the material responsible for the dip was ionized by some other mechanism, such as by collisions.

The X-ray dips occur at phases 0.90–0.15, while the optical emission line absorption dips last between phases 0.0–0.3 (although in non-simultaneous data). The optical dips (Sec-

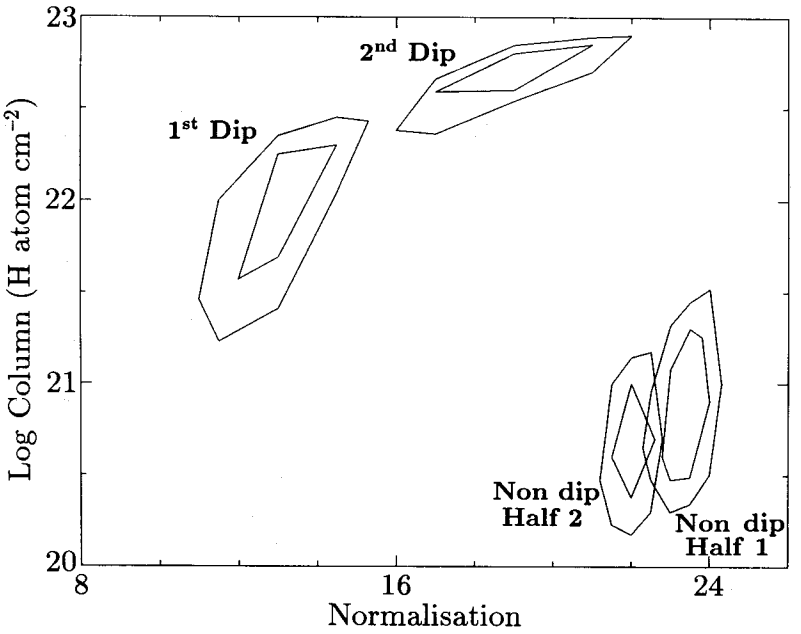

Figure 11. Spectral analysis of the two dips seen in the first 1983 *EXOSAT* observation. One sigma and 90 per cent confidence contours are shown for the two dips and the remaining regions in each half of the ME instrument. The fits used a power law with slope fixed at -0.8.

tion 2.3) are concentrated in the line centre and so originate in low-velocity material (± 200 km s^{-1}). The coincidence in phase suggests a common origin in the material thrown up by the impact of the stream and disc. The greater length of the optical dips could be due to the larger extent of the optically emitting disc, producing back illumination of the material over a greater range of phases.

3.2 The spin cycle

To investigate the relationship between the X-ray and optical spin modulations we have folded the *EXOSAT* data according to the quadratic ephemeris of Kaluzny & Semeniuk (1988, see Section 2.1). The results (Fig. 12) show that the X-ray modulation is largely in phase with the optical. In addition, though, there are significant differences in the X-ray light curves at different energies. The pulse amplitude of the spin variation is a strong function of energy, varying from 100 per cent in the LE data, to ~50 per cent at higher energies. The hardest X-rays show a modulation profile which is flat topped and bottomed and is phased slightly late (phase 0.05). The medium energy X-rays have an asymmetric profile with a faster rise to maximum producing a slightly early peak (0.95). The low-energy data peak later than the medium-energy X-rays, as far as can be determined given the lower statistical quality. These features are stable between the observations. The far right panel in Fig. 12 shows the data during the dips in the 1983 observations folded on the spin cycle. This shows that the spin modulation is still seen with the same pulse fraction but with the overall flux reduced. The extinction is greatest at low energies resulting in no significant signal in the LE band during the dips.

To analyse the spectral variations with the spin cycle we accumulated the X-ray data from the 1985 observations into four intensity bins. The first bin contained data from the quarter cycle at spin maximum (phases 0.875–0.125), the second from the remaining regions of above average flux (phases 0.75–0.875 and 0.125–0.25), the third from phases 0.25–0.375 and 0.625–0.75 and the last from spin minimum (phases 0.375–0.625). The data from the two halves of the ME array were analysed separately and were combined with the LE data. Data from the orbital dip regions were rejected. The spectra covered the range from the low-energy LE cut-off (~0.1 keV) to the limit of adequate statistical quality at 8–9 keV.

We found that all the spectra were adequately fit by a simple power law together with an absorbing column. An alternative was a thermal bremsstrahlung; however, the data did not extend to high enough energy to constrain the temperature and so we preferred the power-law description to minimize parameters. The fits to some of the phase-resolved spectra were improved by the addition of an iron line at 6.7 keV, but the improvement justified the extra parameters in only a few cases; for consistency, therefore, no iron lines were added in the following analysis.

Various models have been proposed to contribute to the spin-period modulations in intermediate polars. These are: (i) energy independent occultation of the X-ray emitting accretion column above the magnetic poles of the white dwarf (King & Shaviv 1984); (ii) the differing line-of-sight absorption through the accretion column over the spin cycle (Rosen, Mason & Córdova 1988; Mason, Rosen & Hellier 1988); (iii) and energy-independent electron scattering (e.g. Buckley & Tuohy 1989). To test these models we have investigated whether the data from all spin phases could be fitted using the same power-law slope and allowing only the normalization and absorbing column to differ. We fitted the spin-maximum data with a free power-law slope and then fixed the slope at this value while fitting the other data obtained with the same ME half on the same day. The results for the two 1985 observations are given in Table 1. Overall, the model provides a good description of the data (the aver-

1991MNRAS.248..233H

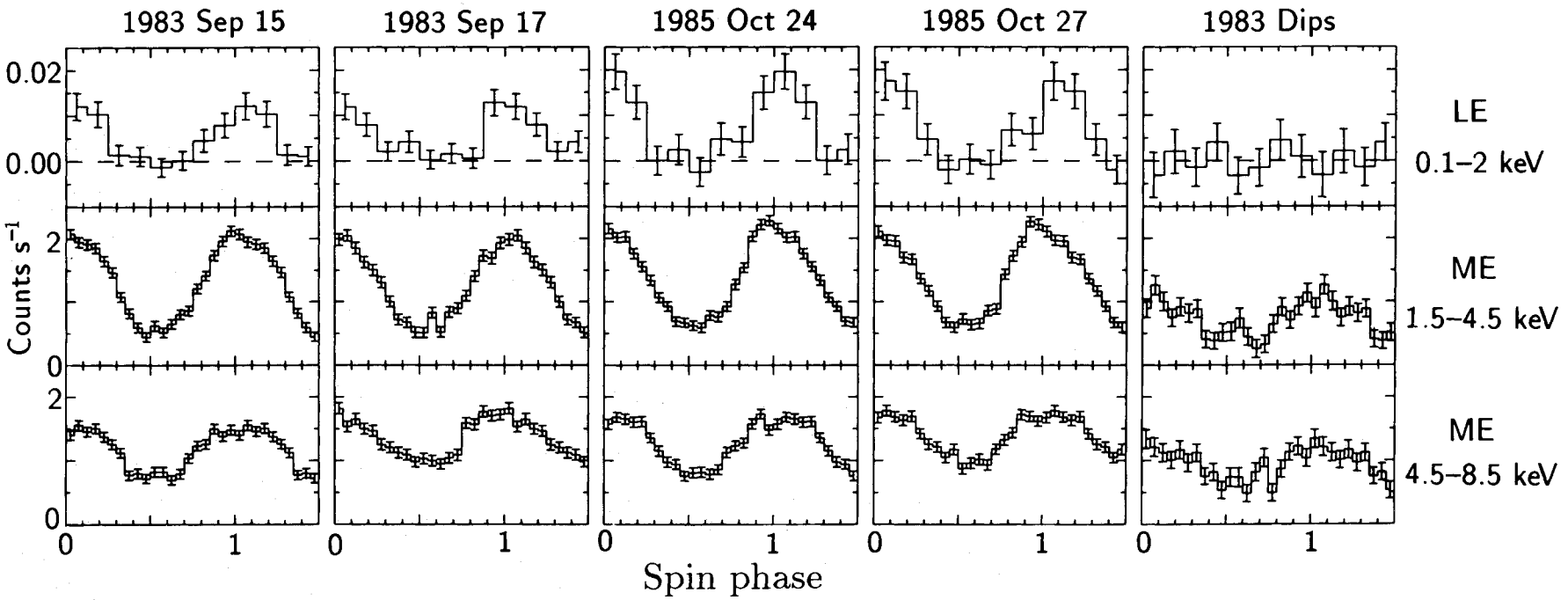

Figure 12. *EXOSAT* data folded on the spin cycle according to Kaluzny & Semeniuk's (1988) quadratic ephemeris. The panels from each observation show the LE (0.1–2 keV), ME 1.5–4.5 keV and ME 4.5–8.5 keV emission. The furthest right panels show the data accumulated during the dips in the 1983 observations.

Table 1. Spin-resolved X-ray spectral analysis.

	Relative normalization	Power law slope	Column (10^{20} H cm^{-2})	χ^2_ν ν=27
Oct 24 Half 1				
Max	1.00	-1.1 ± 0.1	6^{+6}_{-3}	1.27
2nd	0.84	"	40^{+35}_{-20}	1.34
3rd	0.72	"	320^{+140}_{-80}	0.87
Min	0.50	"	470^{+350}_{-200}	0.99
Oct 24 Half 2				
Max	1.00	-1.2 ± 0.1	15^{+10}_{-6}	1.24
2nd	0.75	"	23^{+18}_{-12}	1.29
3rd	0.57	"	103^{+70}_{-40}	0.81
Min	0.42	"	229^{+140}_{-100}	0.97
Oct 27 Half 1				
Max	1.00	-1.0 ± 0.1	3^{+6}_{-2}	0.80
2nd	0.84	"	9^{+14}_{-5}	1.15
3rd	0.67	"	240^{+150}_{-90}	1.35
Min	0.49	"	310^{+160}_{-100}	1.08
Oct 27 Half 2				
Max	1.00	-1.2 ± 0.1	14^{+10}_{-6}	1.02
2nd	0.84	"	30^{+30}_{-10}	1.14
3rd	0.68	"	210^{+100}_{-70}	0.83
Min	0.56	"	390^{+190}_{-100}	0.73

age χ^2_ν obtained is 1.06). Where a poorer fit is obtained, for example in the brighter phases during the October 24 observation, this is due to scatter in the data rather than systematic departures from the model. The results indicate that the X-ray emission can be characterized by a power law with a slope of -1.1, and the spin modulation reproduced by varying the normalization by a factor of 2 and the absorbing column from 5×10^{20} to 5×10^{22} H atom cm^{-2} between spin maximum and spin minimum.

A similar analysis has been performed by Norton & Watson (1989) on the X-ray spectra of all intermediate polars observed by *EXOSAT*; however, they reached a conclusion differing from our analysis of AO Psc. They found that a fixed power law together with variable normalization and column was not adequate to model the spin-resolved spectra but resulted in excess low-energy emission at all spin phases. Their analysis differed from ours in using only two phase bins, high and low, to preserve sufficient statistics in intermediate polars which are weaker X-ray sources than AO Psc. More importantly, they fixed their power-law slope at a value derived from fitting the phase-averaged spectrum, whereas we fit it at a value determined at spin maximum. As the spectrum contains proportionately more low-energy emission at spin maximum, the fitted power law will be steeper. Thus, the excess low-energy emission seen by Norton & Watson may result from their systematically flatter power law. To achieve an acceptable fit, Norton & Watson introduced a more complex absorber which partially covers the source, letting through a fraction of the flux with a lower absorption and so reproducing the low-energy excess (this raises the number of parameters from three to five and achieves χ^2_ν values similar to ours). Our results indicate that, in AO Psc, this is not necessary and that a simple absorber is adequate, at least as far as can be determined with the current X-ray spectra whose statistical quality is only barely adequate for phase resolved analysis.

4 DISCUSSION

To introduce the discussion of our data we briefly summarize the overall picture of an intermediate polar. While the accretion geometry of an AM Her star, or polar, is totally dominated by the magnetic field, in an intermediate polar its effect is reduced by the lack of spin-orbit synchronism combined with a generally wider orbit and a possibly smaller field strength. It is often considered that the magnetic field has little effect at more than $\sim 10^{10}$ cm from the white dwarf and that, further out, an intermediate polar resembles a non-magnetic cataclysmic variable, complete with a Keplerian accretion disc and an impact region (bright spot) where this is struck by the mass-transfer stream from the secondary. Within $\sim 10^{10}$ cm, material is magnetically controlled and corotates with the white dwarf while accreting quasi-radially along the field lines on to the magnetic poles. The two regions are separated by a poorly-understood transition region. This scenario implies that observations of intermediate polars will decouple into orbital-cycle phenomena, giving a picture of the outer regions of the binary, and spin-cycle effects, emanating from close to the white dwarf. X-rays from the spin-dominated region will, though, reprocess off the cooler outer regions to produce an optical modulation at the beat period between the spin and orbital cycles. In addition, at high inclinations, obscuration of the central object by material further out in the binary (as often seen in 'dipping' low-mass X-ray binaries; e.g. Parmar & White 1988) could result in orbital modulations in the X-ray band.

This picture may, however, be oversimplified. Part of the accretion stream from the secondary may overflow the disc and continue to an impact with the magnetosphere (e.g. Mason, Rosen & Hellier 1988; Hellier *et al.* 1989; Lubow 1989). More radically, Hameury, King & Lasota (1986) pointed out that if the magnetospheric radius is greater than the natural circularization radius of the accretion stream, a disc may not be able to form at all; the entire accretion stream would then impact on the magnetosphere (at $\sim 10^{10}$ cm) and fragment into large blobs of material which continue on a ballistic trajectory until threaded by the magnetic field. They suggested that such blobs could travel as far as the white-dwarf surface, producing orbital-cycle phenomena from the 'spin-dominated' regions.

4.1 The orbital phenomena

As a first step we discuss the implications of our data for the phasing and inclination of the binary system and the overall accretion geometry.

The sinusoidal optical-photometric modulation with AO Psc's orbital period probably reflects the varying aspect of a localized, X-ray-illuminated region, such as the secondary or the disc-stream impact region. Minimum light (phase zero with our adopted ephemeris, which may be in error by ~ 0.1, Section 2.1) would occur at inferior conjunction of the region. We can infer the phasing of the impact region in AO Psc by assuming that it produces the orbital cycle *S*-wave (Section 2.3) which is phased with maximum redshift at

$\phi_{orb} = 0.28 \pm 0.03$. As *S*-waves from the impact region generally reflect the local disc (Keplerian) velocity, this implies that inferior conjunction of the impact region occurs at 0.03 ± 0.03, i.e. orbital minimum. However, the ephemeris has an error bar of ~ 0.1. Hence, if the disc nearly fills the Roche lobe, producing an impact region nearly along the line of stellar centres and so phased only slightly ahead of the secondary, then it is possible that orbital minimum actually coincides with inferior conjunction of the secondary. Note, also, that X-ray illumination of both the secondary and the impact region could contribute to the photometric orbital modulation producing a minimum at inferior conjunction of their flux-weighted centroid.

Further information, though, is provided by the X-ray dips recurring at orbital minimum (Section 3.1). During the dips the spin modulation is present in the *EXOSAT* ME data with the same fractional amplitude as away from the dips, while spectral analysis shows an increase in photoelectric absorption in one dip. The 0.1–2 keV (LE) emission is entirely spin modulated away from the dips and is extinguished during the dips (Figs 10 and 12). This implies that we are seeing the central, spin-modulated X-ray source obscured by an absorbing cloud and rules out alternative models such as the occultation of a second X-ray-emitting region. X-ray dips are commonly seen in high-inclination interacting-binary stars and in particular are seen in both of the eclipsing intermediate polars, EX Hya (Córdova, Mason & Kahn 1985) and FO Aqr (Norton *et al.* 1990). In these systems the dips precede the eclipse, occurring at inferior conjunction of the impact region, and may be produced by material thrown up by the impact. Hence, by analogy with these systems, we conclude that the X-ray dips and orbital minimum in AO Psc probably occur at inferior conjunction of the impact region and that inferior conjunction of the secondary occurs later at about phase 0.1 (depending on the disc size).

We can estimate the disc radius by assuming that the disc is Keplerian. The observed semi-amplitude of the *S*-wave (400 km s^{-1}, Section 2.3.1) then locates the distance of the impact region from the primary, though only as a function of the primary mass and the system inclination. Specifically, $r_{disc} = 8.3\ M \sin^2 i$ in units of 10^{10} cm and $M_\odot$. The X-ray dips suggest a moderately high system inclination, but it is not sufficiently high to produce eclipses. Taking $i = 60°$ and $M = 0.8\ M_\odot$ gives $r_{disc} = 5 \times 10^{10}$ cm. For comparison, with a 3.59-hr orbital period, a 0.8 $M_\odot$ primary and a 0.33 $M_\odot$ secondary (from the orbital period–secondary mass relationship of Patterson 1984) the stellar separation is 8.6×10^{10} cm, and the inner Lagrangian point is 6.0×10^{10} cm from the primary.

4.1.1 *The disc-less model*

So far we have assumed the presence of a disc and have concluded that the observed *S*-wave velocity and phasing is compatible with this assumption. We now consider the alternative 'disc-less' proposal of Hameury *et al.* (1986). In this model the *S*-wave is produced by the impact of the accretion stream with the magnetosphere at $\sim 10^{10}$ cm, considerably closer to the white dwarf than in the disc model. At this radius the expected velocity would be greatly increased. The result would most likely be similar to the high-velocity *S*-wave with a late phasing which is seen in EX Hya during outburst, in addition to the usual lower velocity *S*-wave (Hellier *et al.* 1989). To reconcile the expected high velocity with the AO Psc observations would require a very much smaller inclination. Using a 0.8 $M_\odot$ white dwarf, the Keplerian velocity at 10^{10} cm is 1000 km s^{-1}, compatible with the observed velocity of 400 km s^{-1} at an inclination of 23°. If instead, the *S*-wave velocity reflected the local velocity of corotation with the white dwarf (780 km s^{-1}) or the free-fall velocity (1400 km s^{-1}), the inclination would be 31° or 16° respectively. If the magnetospheric radius were much greater than $\sim 10^{10}$ cm, the corotation velocity would dominate, again producing velocities much higher than observed except at very low inclinations.

It is difficult to see, though, how a system at these low inclinations could produce the observed optical-photometric orbital modulation. Furthermore, to produce the X-ray dips by obscuration of the white dwarf, the obscuring material would have to be elevated from the orbital plane by an angle of $\sim 70°$ (measured at the white dwarf) and still produce the well-defined dips seen in Fig. 10.

McHardy *et al.* (1987), following Hameury *et al.* (1986), postulated a second X-ray emitting region to explain similar dips in BG CMi. They suggested that the impact region of the stream at the magnetosphere was itself a soft X-ray source, emitting ~ 10 per cent of the accretion luminosity, and that self-occultation of this region caused the orbital-cycle dips. If this were so, then the spin-modulated emission from the ultimate accretion region on the white dwarf would be largely unaffected. In AO Psc, however, the fact that the low-energy emission is completely spin modulated implies that it originates in one spin-dominated region, and the fact that it is extinguished during the dips implies that it is this region that is being obscured.

Hameury *et al.* (1986) proposed that orbital-cycle X-ray variations could result from material following a ballistic trajectory (largely unaffected by the primary's magnetic field) to the white-dwarf's surface. This would produce an X-ray-emitting region on the white dwarf which is fixed in the binary frame and occulted by the white dwarf itself for part of the orbital cycle (producing an on–off modulation similar to that seen in AM Her stars). While the large blobs produce the orbital variation, material stripped from the blobs becomes magnetically dominated and results in a concurrent spin modulation. Since Hameury *et al.* quote the orbital dips in AO Psc (along with similar effects in EX Hya) as the most persuasive evidence for their disc-less model, we pay particular attention to comparing this model with the observations.

A number of difficulties arise. First of all, the full amplitude of the spin modulation is 75 per cent at 2–4 keV. This places an upper limit of 25 per cent on the fractional luminosity that can result from blobs which escape magnetic permeation. Secondly, as the spin pulse is visible throughout the orbital cycle, the magnetically-dominated material must be spread approximately uniformly in azimuth. Hence, we would expect the spin modulation to be largely unaffected by the orbital phase and continue to be visible while the postulated blob-accretion region is on the far side of the white dwarf. In fact, though, the spin-modulated flux shows a reduction proportional to the overall intensity during the dip, and the low-energy emission is entirely extinguished. This behaviour instead suggests that the dips are caused by photoelectric absorption in an obscuring cloud.

A further problem concerns the phasing of the dips. The X-ray dips are localized to ~0.1 of the cycle and, from reference to the optical data, they occur at inferior conjunction of the impact region producing the orbital-cycle emission-line *S*-wave (Sections 2.3 and 3.1). This phasing is naturally explained if the dips are caused by obscuration by this region. In Hameury *et al.*'s model, the *S*-wave is caused by the impact with the magnetosphere. Hameury *et al.* expect that the large blobs would follow a trajectory of approximately radial infall in the spin-rotating frame from this magnetospheric impact. We can estimate the possible phase shifts by comparing the infall time-scale with the spin period. Combining a magnetospheric radius of 10^{10} cm with a typical free-fall velocity at this radius (~ 1500 km s^{-1}) results in a free-fall time of ~1 min or <0.1 of the spin cycle. Hence, inferior conjunction of the magnetospheric-impact region would nearly coincide with maximum visibility of the blob-accretion region – it is the least likely phase for a dip due to occultation of the region by the white-dwarf surface.

Lastly, the dips are almost absent during the 1985 *EXOSAT* observations. This is easily explained in an obscuration model; such variability is commonly seen in the dipping low-mass X-ray binaries (e.g. Smale *et al.* 1988) and is attributed to turbulence in the disc structure. It could also arise in Hameury *et al.*'s model if turbulence in the magnetosphere affected the efficiency with which material is stripped from blobs; but only if, as a result, little blobby accretion remained. Thus, the absence of the dips in 1985 and the large spin-pulse fraction indicate that blobby accretion is responsible for, at best, a small fraction of the total X-ray flux.

Hence, on the strength of the arguments presented above, we exclude blobby accretion as a major factor. This is important as the accretion geometry greatly affects the area of the white-dwarf surface over which accretion occurs. Accretion from a disrupted disc results in accreting fractional areas of the white-dwarf surface of $f \lesssim 0.01$ (Rosen *et al.* 1988). Disc-less accretion in which blobs are completely dissipated by stripping results in $f \sim 0.05$ (Hameury *et al.* 1986). Only if a significant fraction of the material accretes as blobs able to cross field lines does the accretion fraction increase to $f \gtrsim 0.1$ (Hameury *et al.* 1986). This has important consequences for the origin of the spin pulse itself (see Section 4.2.2).

4.2 The spin-period behaviour

It is now well established that intermediate polar emission lines commonly show radial-velocity variations with the spin period (Hellier & Mason 1990). In the first report of such behaviour, Penning (1985) proposed that it resulted from the reprocessing of an X-ray beam by the disc. The beam, sweeping round with the spin cycle, would illuminate a section of the disc and produce optical emission shifted by the local Keplerian velocity. In this model one would expect that at X-ray flux maximum the beam would predominantly illuminate disc material travelling across the line-of-sight. Thus, the velocity modulation would be phased with zero velocity at X-ray maximum.

In our previous work on EX Hya and FO Aqr (Hellier *et al.* 1987; Hellier, Mason & Cropper 1990), though, we found an emission-line spin variation that was phased with maximum blueshift coincident with optical and X-ray spin maximum. To explain this we placed the source of the spin-varying line emission in the magnetosphere rather than the disc, and we proposed that the observed velocity reflects the quasi-radial infall of material accreting along the magnetic-field lines near to the white dwarf. This model places the velocity vector almost parallel to the projection of the magnetic axis in the orbital plane and so explains the observed phasing.

A similar 'magnetospheric' origin for the velocity modulation of the emission lines in the intermediate polars was proposed by Buckley & Tuohy (1989, 1990) to explain their observations of TX Col (H0542−407) and the suspected intermediate polar TW Pic (H0534−581). Motivated largely by the need to explain the low modulation amplitude measured (20–30 km s^{-1}) they proposed that the observed variation was due to the velocity of corotation with the magnetic field – which is sufficiently low for material at a radius of 2–10 white-dwarf radii in relatively slow rotators such as TX Col and TW Pic. Note that the corotation velocity lags the infall velocity by a quarter of a cycle in phase, allowing a distinction between them if the phasing is known.

4.2.1 *The accretion-curtain model*

To aid the discussion of the magnetospheric model, we illustrate the proposed geometry in Figs 13 and 14. While in the disc, the accreting material circulates at the local Keplerian velocity. It then encounters a boundary layer where its velocity changes to quasi-radial infall along the field lines on to the magnetic poles. The production of a spin pulse requires that the magnetic axis be offset from the spin axis. This asymmetry allows preferential accretion along field lines around the region of the disc at which the magnetic pole points. Material will connect on to field lines over a range of azimuth, forming an azimuthally extended, arch-shaped accretion curtain of material which rises out of the disc plane before falling on to the magnetic pole, where it has an arc-shaped footprint on the white-dwarf surface (see Rosen *et al.* 1988 for a fuller account). In AM Her stars, the material approaching the magnetosphere has an infall velocity which might enable it to overcome the gravitational potential barrier to accretion on the second pole. When accreting from a disc, though, material from each disc half is more likely to be limited to accreting on to the pole pointing towards it.

To make a simple estimate of the velocity of the material in the curtain we assume that the material approaching the boundary layer is in a Keplerian orbit with zero infall velocity. From here, if we ignore turbulence, the kinetic energy of infall increases in proportion to the change in gravitational potential along the field lines. The material initially travels relatively slowly, speeding up as it approaches the apex of the arch, and then accelerates rapidly from the apex to the white-dwarf surface in virtual free fall. The speeds obtained will be a function of the white-dwarf mass, the dipole offset angle and the radius of disc disruption. Fig. 15 illustrates the speeds expected for material following two particular field lines. In addition to the infall velocity, the material will have a velocity of corotation with the magnetosphere. This is 90° out of phase with the infall velocity and increases linearly with radius; illustrated in Fig. 15 for the particular case of AO Psc's spin period.

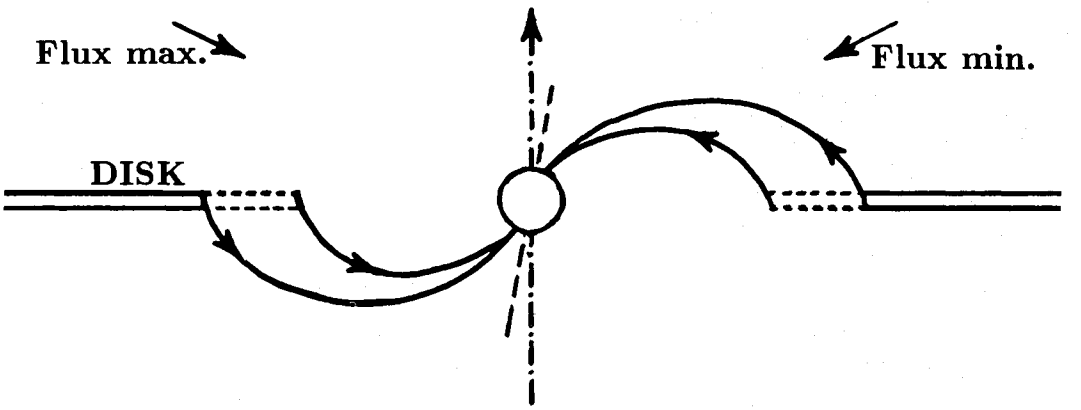

Figure 13. A side view illustrating the 'accretion-curtain' model of an intermediate polar. The magnetic field disrupts the disc over a range of radii forcing material to follow the field lines on to the white dwarf. Maximum visibility of the inner regions of the curtain occurs when the upper pole points away from the observer – this causes optical- and X-ray flux-maximum.

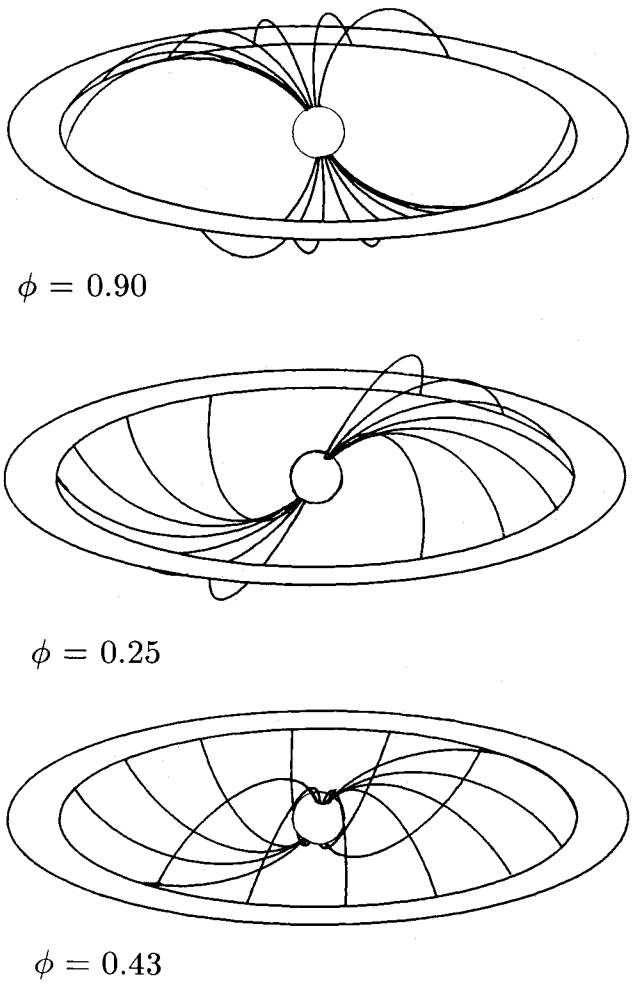

Figure 14. A three-dimensional illustration of the accretion curtains falling to the magnetic poles of an intermediate polar. The arch-shaped accretion curtain is azimuthally extended and has a footprint on the surface forming an arc around the magnetic pole covering only $\lesssim 1$ per cent of the white-dwarf surface area. The variations in our view of the curtain with spin phase explain the spin-period behaviour of the X-rays, optical continuum and emission lines in intermediate polars. Spin-flux maximum (phase zero) occurs when the upper pole points away from the observer.

The calculations in Fig.15 are for free fall along a particular field line. Several further factors need to be taken into account in extending the calculation to the full accretion curtain. These will all lower the velocities from those shown in Fig. 15.

(i) Turbulence in the accretion flow will dissipate energy and reduce the velocities.

(ii) The observed emission lines will come from a spread of azimuth with varying velocity projections on to the line-of-sight. This will dilute any velocity variation.

(iii) The surface area of the accretion curtain is weighted to the lower velocity outer regions (Fig. 14). If the emission is uniform and optically thick, the observed line profiles will be similarly weighted to low velocities.

(iv) The effective dipole offset decreases with azimuth from the centre of the curtain, lowering the velocities at large radii.

(v) If the white dwarf is spinning slower than the equilibrium rate (AO Psc is spinning up; van Amerongen *et al.* 1985) the field lines near the boundary layer will be swept up by the disc material and pulled ahead of the radial position illustrated in Fig. 14. Material following field lines will therefore be travelling against the corotation with the magnetosphere and the two velocities will tend to cancel.

With this situation, a full comparison with the observations requires a complex model of the emission lines from an accretion curtain. In this paper we attempt a more qualitative comparison and postpone the necessary modelling to future work.

4.2.2 *The spin-varying line emission*

We first summarize the spin-varying features of the emission lines of AO Psc and then interpret them using the magnetospheric-curtain model.

The broad velocity-modulated 'spin-wave' is phased, as was that of FO Aqr, with maximum blueshift at optical and X-ray spin maximum (actually phase 0.95 ± 0.03). It has a width of 450 ± 50 km s^{-1} (FWHM) and a semi-amplitude of 260 ± 30 km s^{-1}. Its mean (γ) velocity can be estimated by its difference from that of the orbital S-wave (which presumably has a mean velocity equal to the systemic velocity). This gives

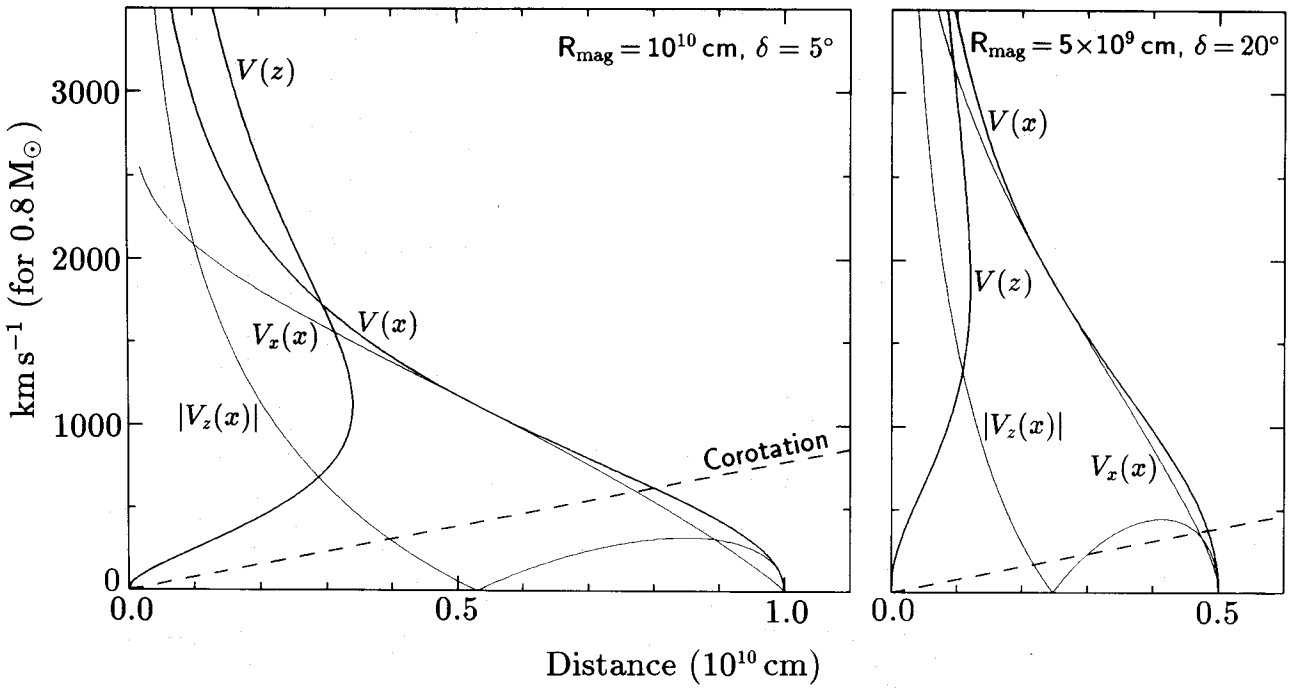

Figure 15. Simplistic calculation of the velocities expected following a particular field line in the accretion curtain. The left-hand panel assumes a magnetospheric radius of 10^{10} cm and a dipole offset of 5°, while the right-hand panel assumes a radius of 5×10^9 cm and an offset of 20°. The thicker lines show the total speed as a function of distance from the white dwarf in the plane (x) and out of the plane (z). The thinner lines show the velocity components in the x and z directions as a function of x. Also shown (dashed) is the corotation velocity for AO Psc's spin period. The velocities scale as the square root of the white-dwarf mass; in the figure we have assumed a mass of 0.8 $M_\odot$.

-40 ± 43 km s^{-1} (Sections 2.3 and 2.4). The He II λ4686 line also contains a narrower component. This has a FWHM of 125 km s^{-1}, no velocity variation with a limit of 70 km s^{-1} and a γ shift of -25 ± 42 km s^{-1}. It also varies in flux and equivalent width by a factor of 3 over the spin cycle.

These measured velocities depend on the chosen Gaussian decomposition being an accurate reflection of the line components. The spin-folded line profiles will contain averaged profiles from emission not varying with the spin cycle (the variation of the He II λ4686 line with the orbital and beat cycles shows that such emission is present). These components, which are stationary when folded on the spin cycle, will dilute the amplitude of any spin-cycle velocity variation and hence the values quoted above are likely to be underestimates of the true values for the spin-varying emission.

Converting the measured semi-amplitude and mean velocities to components perpendicular to and in the orbital plane is of course dependent on the system inclination. This is uncertain, but the orbital behaviour (X-ray dips but no eclipses, Section 4.1) suggests ~60°.

All current models for the X-ray spin pulse place maximum flux when the projection of the magnetic axis in the disc plane lies along the line-of-sight, either pointing toward or away from the observer (Section 4.2.3). The phasing of the spin-wave is therefore consistent with the origin of the velocity being the quasi-radial motion down the accretion curtain. As with EX Hya and FO Aqr, the blueshift at flux maximum implies that the predominantly observed (upper) pole points away from the observer at this phase. This phasing also implies that the infall velocity dominates over the velocity of corotation, which is phased a quarter of a cycle later. As the corotation velocity increases linearly with radius this limits the distance from the white dwarf of the region emitting the spin-wave. For an 805-s spin period and an inclination of 60°, 260 km s^{-1} is the projected corotation velocity at 4×10^9 cm (~7 white-dwarf radii), implying that the emission originates within this radius. This limit would be increased if the field lines were swept up by the disc and no longer radial. As mentioned above, the non-radial component of the motion along field lines would then tend to cancel with the corotation velocity and produce a more radial inflow.

The spin-wave produces pronounced asymmetries in the line profiles (Plate 2). This implies that we are seeing emission predominantly from only one pole in contrast to EX Hya where emission from material falling on to both poles produce anti-phased velocities and hence a much more symmetric profile (Hellier *et al.* 1987; Hellier & Mason 1990). The marginal blueshift of the spin-wave ($\gamma = -40 \pm 43$ km s^{-1}, with a 90 per cent limit of -100 km s^{-1}) implies that its velocity is parallel to the orbital plane or rising slightly out of it. The limit on γ of 100 km s^{-1}, combined with the observed semi-amplitude of 260 km s^{-1} and an inclination of 60°, limits the velocity vector's angle to the plane to less than 34°. We therefore identify the spin-wave with emission from material with a flux-weighted centroid approaching or at the apex of the arch of the upper accretion curtain (Fig. 14). Material near the apex is visible throughout the cycle and so would produce a spin-wave prominent throughout the cycle, as observed in He II λ4686 (Plate 2).

A problem with this model, though, is that our simplistic calculation shown in Fig. 15 predicts velocities higher than those observed. At an inclination of 60° the spin-wave amplitude corresponds to a true space velocity of 300 ± 35 km s^{-1}. From Fig. 15, material between the point where it travels

at less than 34° to the plane, and the apex, has velocity in the range 500–1500 km s^{-1}. However, as mentioned above, the corrections to Fig. 15 to account for the complexity of the real situation will all tend to lower the expected velocities, while the observed values are likely to be lower limits. Since the velocities scale with the square root of the white-dwarf mass, we could also postulate a lower mass than the 0.8 $M_\odot$ assumed in Fig. 15. If these effects do not reduce the velocities by the required amount (a factor of ~2), we would then be forced to an inclination lower than 60°, thus lowering the projected velocities. However, this would produce difficulties in understanding the orbital behaviour (principally the X-ray dips, see Section 4.1). It is clear that more detailed modelling is needed to determine whether these effects are sufficient to reconcile the expected velocities with those observed.

The narrow component of the He II λ4686 line shows no detectable velocity modulation, yet it varies by a factor 3 in flux with the spin cycle, being faintest at spin maximum. This implies that it originates in or near the magnetosphere – if it were further from the white dwarf we would expect it to be fixed in the binary frame and any modulation would then occur with the orbital or beat cycles. In our magnetospheric model, the lowest velocities occur just within the boundary layer where the material is beginning its radial infall. This location also explains the flux modulation since the low-velocity regions near the boundary layer are readily visible at spin minimum but obscured by the accretion curtain near spin maximum (Fig. 14).

As the infall velocity is low, the dominant velocity at this location will be the corotation velocity. At first sight, the limit on the observed velocity modulation rules out this model by requiring that it occurs unreasonably close to the white dwarf (within half a white-dwarf radius of the surface). Again though, there are several factors which could account for its absence. If the emission is optically thick (proportional to projected area) the emission will be heavily weighted to the regions nearest the observer which travel across the line-of-sight. If material leaving the plane toward the lower pole is visible, this will have the opposite velocity to material travelling upwards, producing a null resultant and broadening the line. These outermost regions of the magnetosphere will also be the most affected if the field lines are swept ahead of the radial position by the disc, causing the infall velocity to partially cancel with the corotation velocity. Possibly more important is that our measurement of the velocity modulation of the spin-varying narrow component will be diluted by any additional components. The modulation of the centre of the He II λ4686 line with the beat period (Plate 2) implies that there is an additional component from a region fixed in the binary frame.

A further consideration for this model is the width of the narrow component. The boundary layer between the disc and the magnetosphere might be expected to be turbulent due to the rapid change from circular motion to quasi-radial infall. However, since the narrow component has an FWHM of 125 km s^{-1} our model requires that any turbulence be less than this value.

We conclude that the outer edge of the magnetosphere provides a plausible location for the narrow component, possibly the only plausible location as it is difficult to conceive of any other producing emission with a low-velocity modulation yet with a pronounced spin-period flux modulation.

We have proposed, largely because of the low velocities, that the region emitting the He II λ4686 line in AO Psc lies before the apex of the accretion curtain and noted that this explains the flux modulation of the line (it has a minimum at X-ray flux maximum, when the regions before the apex are obscured by the curtain; Fig. 14). The Balmer lines in AO Psc show little variation in equivalent width with spin phase, suggesting that they originate nearer the apex of the arch which is equally visible at all spin phases. It is interesting to note that in EX Hya, where the high velocities (up to 3500 km s^{-1}, Hellier *et al.* 1987) imply a location nearer the white dwarf than the apex (Fig. 15), the emission-line flux is *greatest* at X-ray maximum – which corresponds to maximum visibility of the regions *past* the apex. We have also proposed this mechanism (Hellier *et al.* 1990) to explain the flux modulation of the spin-wave in FO Aqr. Here again, the velocities are higher than in AO Psc and the line fluxes are modulated to a greater extent than the continuum.

We have seen that the phasing of the spin-wave indicates that the infall velocity dominates over the corotation velocity, and that this limits the distance of the emission region to less than 4×10^9 cm from the white dwarf. This, in turn, locates the magnetospheric radius at no more than $\sim 5 \times 10^9$ cm (~8 white-dwarf radii). Using the standard formula for disc accretion (e.g. King, Frank & Ritter 1985) together with $\dot{M} \sim 10^{17}$ g s^{-1} and $M_1 \sim 0.8$ $M_\odot$ then gives a magnetic moment of $\mu \sim 0.16 \times 10^{33}$ G cm^3 which corresponds to $B \sim 0.7$ MG. This estimate of the magnetic field is more than an order of magnitude below those commonly measured in AM Her stars (see Cropper 1990) which suggests that the two classes are separate populations rather than different evolutionary stages of the same population. Very similar estimates of the magnetospheric radius and magnetic moment were made for TX Col by Buckley & Tuohy (1989) and EX Hya by Hellier *et al.* (1987).

To summarize our discussion of the spin-varying line emission we conclude that the accretion-curtain model provides a good qualitative explanation of the variations. However, further work is needed to demonstrate that the observations are quantitatively compatible with the model.

4.2.3 *The X-ray spin modulation*

All studies of the X-ray spin-period modulation in intermediate polars agree that an increase in photoelectric absorption is an important factor (Rosen *et al.* 1988; Norton & Watson 1989; Section 3.2). In our analysis, the absorbing column changes by two orders of magnitude from 5×10^{20} to 5×10^{22} H atom cm^{-2} between flux maximum and flux minimum. However, we found that an additional reduction in normalization by a factor 2 was required to model the modulation. A requirement for an energy-independent modulation was also reported by Norton & Watson (1989) in their survey of the *EXOSAT* data from all intermediate polars. This energy-independent contribution is in phase with the energy-dependent modulation. Two different explanations for these results have been proposed, each requiring a very different accretion geometry.

The geometry proposed by Rosen *et al.* (1988) is essentially that which we have adopted in explaining our optical data as illustrated in Fig. 13. The accreting material follows

field lines inwards from the magnetospheric radius, forming an accretion curtain with a shape analogous to an auroral arc. The footprint on the stellar surface is an azimuthally extended narrow arc around the magnetic pole totalling a fractional area, $f \sim 0.001$–0.01 of the stellar surface (depending on the radius of disc disruption and the range of radii over which magnetic threading occurs). Hence, the accretion curtain is tall compared to its cross-sectional area. The major accretion shock occurs above the white-dwarf surface (within one white-dwarf radius) and hard X-rays are emitted by bremsstrahlung in the post shock region. The emitted X-rays encounter most material when travelling upwards in the curtain, through pre-shock material, or along the arc (constant magnetic latitude). In contrast, X-rays emitted normal to the surface of the curtain (constant longitude) will encounter very little material and hence least photoelectric absorption. In the general case of an offset magnetic dipole, our view of the curtain will alter with spin phase, producing the observed spin pulse. Flux maximum will occur when the upper pole points away from the observer and most surface area of the curtain is displayed (Fig. 14).

Buckley & Tuohy (1989) have adopted the same tall, thin accretion curtain in their model for TX Col. They have extended the accretion-column model of Imamura & Durisen (1983) to an intermediate polar and concluded that electron scattering in the accretion curtain can produce the energy independent component of the modulation. In a tall, thin curtain, X-rays are scattered preferentially through its sides; an effect which is naturally in phase with the photoelectric-modulation contribution, as required by the observations. Buckley & Tuohy conclude that the effect of electron scattering is sufficient to beam hard X-rays through the curtain sides provided that the ratio of accretion luminosity to accreting-area fraction, $L/f \gtrsim 10^{36}$ ergs s^{-1}, requiring $f \lesssim 0.01$. Note that the 'tall, thin column' X-ray model, which predicts maximum flux when the upper magnetic pole points away from the observer, is consistent with our interpretation of the optical emission-line spectra where the blueshift at spin maximum also implies this phasing. As the optical-continuum spin pulse is in phase with the X-ray pulse, this opens the possibility of a general mechanism for the intermediate polar spin modulation in all wavelength bands. We discuss this further in Section 4.3.2.

A further modulation mechanism occurs in the accretion-curtain model if emission from the lower pole is also seen. Note that to first order the aspect of the lower pole is the same as that of the upper pole at all phases; modulation effects due to photoelectric absorption and electron scattering are therefore in phase at the two poles. A modulation can occur, however, through occultation of the lower pole by the white dwarf. This will produce an energy-independent modulation which will, again, be in phase with the photoelectric absorption and electron-scattering effects. Note that this effect depends on the X-ray-emission region being above the white-dwarf surface so that regions at both poles are visible simultaneously; otherwise, by symmetry, the disappearance of one pole is matched by the appearance of the other. This also implies that occultation effects cannot produce a modulation out of phase with the other contributions, for instance, through the upper pole disappearing over the limb near flux maximum, as this would be compensated for by the appearance of the lower pole.

Occultation of the lower pole is likely to be most significant in systems with the largest stand-off shock height. EX Hya, with probably the lowest accretion rate among the intermediate polars (~ 10 per cent of that in systems above the period gap), will have the largest shock height (~ 1 white-dwarf radius, Rosen *et al.* 1988) while there is also good evidence that we see X-ray emission from both poles (e.g. Mason & Rosen 1990). Occultation of the lower pole may be particularly important in explaining the hard X-ray spin pulse in EX Hya, since the low accretion rate implies that electron scattering is less likely to be significant.

The alternative, and radically different, accretion geometry for intermediate polars is the 'short, fat' column originally proposed by King & Shaviv (1984). Their model was motivated by the need to reproduce quasi-sinusoidal spin-pulse profiles at a time when there was little evidence of the prominent energy dependence due to photoelectric absorption now known to be ubiquitous in intermediate polars. They suggested that the only plausible mechanism was occultation by the white-dwarf surface. To produce predominantly sinusoidal light curves this requires, first, that the polecaps are large ($f \sim 0.25$), and secondly, that there is a pronounced asymmetry between the two poles to prevent their effects from cancelling (King & Shaviv 1984). Norton & Watson (1989) extended this model after the realization of the role of photoelectric absorption, and deduced that for the absorption effects to be in phase with the occultation required $f \gtrsim 0.1$ and, further, that the magnitude of the absorption required $f \gtrsim 0.3$. Maximum flux in this 'large polecap' occurs when the dominant, upper pole points towards the observer, which is the opposite to that proposed in the 'accretion-curtain' model. When the pole points away from the observer, part of the large polecap disappears over the limb, while the line-of-sight absorption, summed horizontally through the polecap, is greatest. Note that for the occultation to be in phase with the absorption component, this model requires that the accretion occurs over the large area (a 'filled' polecap). A hybrid model involving an arc surrounding a large area (a 'hollow' polecap) is not tenable since occultation and absorption effects would be anti-phased.

It is not clear, in this model, what causes the obscuration of the lower polecap required to break the symmetry and produce a spin modulation. King & Shaviv suggest as candidates either the disc or parts of the accretion flow on to the polecaps. However, in order to obscure the bottom pole at our preferred inclination for AO Psc of 60°, the disc would have to extend well within one white-dwarf radius of the surface, and in any intermediate polar with a lower inclination the disc would have to extend even nearer the white-dwarf surface. If discs do not extend this far, then the accretion flow on to the poles would have to be capable of occulting hard (20 keV) X-rays over the large area of a polecap. However, the observed absorbing columns in the accretion flow are insufficient by two orders of magnitude – indeed it was the belief that the accretion flow could not occult hard X-rays that motivated the occultation model and therefore large polecaps (King & Shaviv 1984). This problem for the occultation model is enhanced by the current consensus that in EX Hya we are indeed seeing hard X-rays from the lower pole (Beuermann & Osborne 1988; Mason & Rosen 1990).

The occultation model requires that hard X-ray-emitting accretion at a polecap occurs over $\gtrsim 0.3$ of the white-dwarf surface area (Norton & Watson 1989), and further, that emission from this area dominates the hard X-ray light curve. It is clear that even if the intermediate polar is 'disc less', this can only occur if the dominant accretion mode involves large blobs which hit the white dwarf before being disrupted by the magnetic field; even disrupted blob accretion results in $f \sim 0.05$ (Hameury *et al.* 1986). Blobby accretion, though, may still be unable to achieve $f \gtrsim 0.3$, Hameury *et al.* do not claim more than $f \gtrsim 0.1$.

Blobby accretion, unaffected by the magnetic field, implies that the accretion is ballistic (fixed in the orbital frame). In our discussion of ballistic accretion (Section 4.2.2), however, we concluded that this accretion mode was not occurring, it being at most an unobserved, small fraction of the total. Even if ballistic accretion were occurring and produced large enough accretion regions, it still could not produce the spin modulation. There is no longer a requirement to hide one polecap as the accretion is determined by the stream from the secondary (producing one accretion region), rather than the magnetic field (producing two). However, this region is fixed in the binary frame, not the spin frame, so the modulation due to its occultation would be at the orbital period, not the spin period. As can be seen directly in the *EXOSAT* light curves (Fig. 10), the dominant modulation is at the spin period, particularly in the 1985 data, where it is hard to discern any orbital effects at all.

A further problem for the large-polecap model relates to the prominent blueshift of the emission lines at spin maximum (Plate 2; Section 2.4). In this model, maximum flux occurs when we look face on at the accretion region and the accretion flow is most directly away from us. It is difficult to conceive of an explanation for the emitting material being predominantly blueshifted at this phase.

In conclusion, summarizing this section and Section 4.1.1, the 'accretion-curtain' model naturally explains the X-ray data, but the 'large-polecap' model faces serious problems when confronted with the observations. This conclusion in favour of the accretion-curtain model implies that occultation of the upper pole by the white dwarf does not contribute significantly to the normal, sinusoidal modulation of intermediate polar X-ray light curves since any contribution would be anti-phased with the other effects. In a particular case it could be argued that the dipole offset is small enough that the upper pole does not disappear over the limb. However, as similar arguments apply to all intermediate polars, in general, X-ray emission must be visible from both polecaps with similar intensity – so that the disappearance of one pole over the limb is compensated for by the appearance of the other. Hence, at least one pole is always visible. With a significant shock height, though, both poles may become visible at spin maximum producing a modulation in phase with the accretion-curtain modulation.

In the accretion model, since the contributions to the spin pulse from both poles are in phase, there is no straightforward way of distinguishing emission from the two poles. Only in EX Hya, where the eclipse provides a sensitive spatial probe of the emission regions, has this distinction been possible so far (Beuermann & Osborne 1988; Mason & Rosen 1990). In this system, the data are indeed consistent with equal flux at the two poles. An equal flux from both poles requires that accretion rates on to both poles are similar, which is most readily achieved if the poles are fed from an accretion disc. In this case, asymmetries such as a dipole offset from the white-dwarf centre have little effect at the radius where material threads on to the field lines.

4.3 The optical-continuum spin pulse

So far we have discussed the interpretation of our results from AO Psc and arrived at a picture of the accretion flow which can explain much of our observations of this star. We now proceed to a comparison with other systems in an attempt to explain both the similarities and the differences between intermediate polars. In doing so we will extend our discussion of the accretion-curtain model, which so far has concentrated on the line emission, to the optical-continuum emission.

4.3.1 A comparison with FO Aqr

Intermediate polars can be divided into two types; those whose optical light curve is dominated by a modulation at the spin period (e.g. FO Aqr, EX Hya and BG CMi), and those which instead show a dominant modulation at the beat period between the spin and orbital periods (e.g. AO Psc, V1223 Sgr and TX Col). As examples of the two types we take AO Psc, the subject of this paper, and FO Aqr [see our recent study, Hellier, Mason & Cropper (1990), and references therein].

AO Psc and FO Aqr have similar orbital periods (3.59 and 4.85 hr, respectively) and similar spin periods (13.4 and 20.9 min). FO Aqr has a slightly higher inclination, 70° compared to our estimate of ~60° for AO Psc. The systems also have comparable optical beat-period amplitudes, 17 per cent for FO Aqr and 8 per cent for AO Psc. The principal difference is that while the optical spin-pulse amplitude in AO Psc (3 per cent) is typically half that of the beat pulse, in FO Aqr the spin pulse has an amplitude of 43 per cent and so dominates the light curve. This photometric difference is not, though, reflected in the behaviour of the emission lines which is remarkably similar between the two stars. Comparison of Hellier *et al.* (1990), fig. 2 with Fig. 2 from this paper shows that the principal V/R variation of all lines is at the spin period in both systems. The He II $\lambda 4686$ line exhibits a prominent spin-period equivalent-width variation in both systems, together with smaller modulations at the orbital sidebands, while the Balmer lines show little equivalent-width variation on either spin or beat periods. The similarities continue when comparing the line-profile variations on the spin period [Plate 2 and plate 2 of Hellier *et al.* (1990)]. The emission lines from both stars show the broad spin-wave feature with the same phasing, maximum blueshift at optical and X-ray spin maximum. The main difference is that in FO Aqr, the spin-wave shows larger variations in equivalent width through the cycle. In both systems, also, we have concluded that accretion occurs via an accretion disc.

Hence, one model can explain both FO Aqr and AO Psc provided that it addresses the only substantial difference in their behaviour – the large optical spin pulse in FO Aqr which is a factor of 10 stronger than in AO Psc.

4.3.2 *The origin of spin-pulsed optical emission*

While it is agreed that the spin-modulated X-ray emission originates close to the white dwarf, the location of the region emitting the optical-continuum spin pulse is more uncertain. Warner (1985) proposed that this region is the whole disc. If the X-ray beam were sufficiently collimated, then reprocessing in the disc coupled with a front–back asymmetry in our view of the disc (as occurs, for instance, with a flared disc at high inclinations) would produce an optical pulse. With the current models for the X-ray emission, though, it is doubtful whether the X-ray emission is sufficiently confined to produce a large optical pulse by this method (a 40 per cent modulation is seen in FO Aqr). With X-rays being emitted through the sides of the accretion curtain, as illustrated in Fig. 13, illumination of both near and far sides of the disc can occur simultaneously. Therefore, although this mechanism may make a contribution, we also consider alternatives.

One possibility is that the region around the polecap is heated by X-rays producing optical emission. Occultation by the white dwarf could modulate this emission if the lower pole were hidden to break the symmetry. However, this would produce minimum flux when the upper pole points away, at X-ray spin maximum, which is the opposite to the observed phasing. Obscuration of the heated polecap by the accretion curtain, however, would be in phase with the X-ray pulse. Occultation need not reduce the amplitude of this modulation if the heated surface were visible at both polecaps at spin maximum. This effect may again contribute to the optical-continuum spin pulse. However, we now discuss some results from EX Hya, where the eclipse allows a spatial probe of the emission regions, which lead us to conclude that the dominant region emitting the optical spin pulse is actually the accretion curtain.

The eclipse in EX Hya (even in X-rays) is partial and very narrow, implying a grazing eclipse of the emitting regions. Observations in the X-ray band indicate that we see X-ray emission from both poles and that only the lower pole is eclipsed (Beuermann & Osborne 1988; Mason & Rosen 1990). The optical eclipse is similarly partial (~ 30 per cent), narrow and coincident with the X-ray eclipse. The amount of flux eclipsed is correlated with the spin phase. These facts imply that spin-modulated emission is being eclipsed and that this emission originates close to the white dwarf. Even more importantly, the times of optical eclipse show a systematic variation about the mean as a function of spin phase (Jablonski & Busko 1985; Siegel *et al.* 1989). This implies that the optical-continuum emission originates inside the magnetosphere and is locked to the white dwarf. The amplitude of the eclipse-time variation corresponds to a location of 1.5×10^9 cm from the white dwarf (2–3 white-dwarf radii; Seigel *et al.* 1989). It is therefore straightforward to identify this emission region with the accretion curtain falling on to the white dwarf. Note that Hellier *et al.* (1987) deduced that line emission also originated from the curtain in EX Hya and, from the observed velocities, concluded that it must also originate within 1.6×10^9 cm. Again, in Section 4.2, we have explained the AO Psc spin-wave by placing it within $\sim 3 \times 10^9$ cm. The phasing of the observed variation in eclipse times in EX Hya agrees with this model.The eclipses are late in the half cycle after spin maximum. The lower (eclipsed) pole points towards us at spin maximum; hence, assuming prograde rotation, the curtain falling to this pole will be eclipsed late following spin maximum.

This leads us to adopt the model we originally proposed for EX Hya (Hellier *et al.* 1987). The optical modulation is simply produced by the varying aspect of the optically thick accretion curtain in the same way as the X-ray modulation (although the optically emitting regions are likely to be located further up the accretion flow than the X-ray emitting base). This proposal has the merit of explaining why the modulations in the two bands are always in phase and have similar profiles. As the emission-line pulse also originates in this region it will again have the same phasing, as is observed.

We have already discussed (Section 4.2.2) the consequences of the accretion-curtain model for the line-emission. Variations in the location of the emission along the curtain alter the modulation amplitude from a large pulse in phase with the X-ray modulation, to a pulse anti-phased (negative amplitude) with the X-ray variation. These considerations will also apply to the optical-continuum emission. The nearer the flux-weighted centroid of the emission is to the white dwarf, the greater will be the variation in our view of this region with spin phase and therefore, the greater the amplitude of the observed spin pulse.

Hence variations in the accretion rate, magnetospheric radius and dipole offset, which all affect the locations of the emitting regions in the accretion curtain, can produce different amplitudes of spin pulse. If the continuum emission in AO Psc is similar to the line emission and originates near the apex of the arch, then the low pulse amplitude is explained. Additionally, the observed amplitude will depend on the system inclination. The variation in our view of the lower regions of the accretion curtain will be greatest at high inclination, while no variation would be expected in a face on system. Hellier & Mason (1990) tabulate the spin-pulse amplitudes and probable inclinations of the known intermediate polars, and show that the two are correlated, as expected with our model. The amplitude of the beat-period pulsation, though, shows little evidence for such a correlation indicating that its magnitude is more probably governed by departures from orbital axi-symmetry in the system and hence by the effects of reprocessing. The X-ray spin-pulse amplitudes do show the correlation with inclination expected in our model, but to a lesser degree than the optical pulses. This probably reflects the location of the X-ray emission very close to the white dwarf where the variations in obscuration with spin phase are most pronounced and so least affected by inclination.

We conclude that the spin-varying X-ray, optical-continuum and line-emission components all come from the accretion curtain, and that variations in the emitting location within the curtain, together with variations in the observed inclination, can explain the different spin amplitudes observed in different intermediate polars.

4.4 The energy balance

The final issue we discuss is the energy balance of AO Psc. This was first raised by Hassall *et al.* (1981) who suggested that the EUV/XUV and the X-ray band beyond 10 keV must contain up to 100 times the observed flux in the 2–10 keV range in order to account for the optical/UV luminosity. With our model, the constant and spin-pulsed contributions

to the optical luminosity are not the result of X-ray reprocessing. Therefore, instead, we consider only the flux required to produce the beat-period pulse. The observed flux in the range 1200–7500 Å is 2.5×10^{-10} erg cm^{-2} s^{-1} (Hassall *et al.* 1981), while the beat-pulse fraction is ~8 per cent, giving $\sim2\times10^{-11}$ erg cm^{-2} s^{-1}. The efficiency of production of the beat pulse is unknown, depending on the size of the disc bulge and the degree of X-ray beaming. If we assume that ~10 per cent of the EUV/X-ray flux results in the optical/UV beat pulse then we require $\sim2\times10^{-10}$ erg cm^{-2} s^{-1} beyond the UV. This compares with a 2–10 keV flux observed by *EXOSAT* of $\sim5\times10^{-11}$ erg cm^{-2} s^{-1}. Thus the energy required in the EUV/XUV and in X-rays harder than 10 keV is ~three times that seen in the 2–10 keV range. This implies a total observed luminosity (optical to X-ray) of $\sim5\times10^{-10}$ erg cm^{-2} s^{-1}. For a distance d this corresponds to a total accretion luminosity of $(d/420\ \mathrm{pc})^2\times10^{34}$ erg s^{-1}. A distance of 420 pc is similar to that of GK Per, the only intermediate polar with a well-determined distance (525 pc, Duerbeck 1981). AO Psc also has a similar 2–10 keV flux to that of GK Per [observed in quiescence as 2.7 and 4.5×10^{-11} erg cm^{-2} s^{-1} on two occasions (Norton, Watson & King 1988)]. Combining the observed fluxes with the above distances implies that both objects have a 2–10 keV luminosity of 10^{33} erg s^{-1}.

5 CONCLUSIONS

We have analysed three nights of optical spectroscopy and four *EXOSAT* X-ray observations of the intermediate polar AO Psc. We conclude the following.

(i) Accretion on to the white dwarf occurs via an accretion disc which extends from ~8 white-dwarf radii ($\sim5\times10^9$ cm) to the limit of the Roche lobe ($\sim5\times10^{10}$ cm). This implies that the surface magnetic field, $B\sim0.7$ MG. The impact region of the mass-transfer stream with the disc is at inferior conjunction at orbital photometric minimum. This region produces an orbital emission-line *S*-wave and also the beat-period photometric modulation (by reprocessing).

(ii) Dips seen in the X-ray light curves and the emission lines at orbital minimum are caused by obscuration of the emitting regions near the white dwarf by material above the disc plane at the impact region on the edge of the disc. We exclude alternative models such as self-occultation of a second X-ray-emitting region at the magnetosphere, or occultation by the white-dwarf surface of an accretion region fixed in the binary frame and produced by ballistic 'blobby' accretion (Hameury *et al.* 1986; McHardy *et al.* 1987). The X-ray dips imply a moderately high inclination of ~60°.

(iii) Accreting material is magnetically controlled inside ~8 white-dwarf radii and accretes along field lines, forming 'accretion curtains' of material falling on to each pole. The curtain's footprint is a narrow arc around the pole with an area of $\lesssim0.01$ of the white-dwarf surface. We exclude alternative geometries involving accretion on to large polecaps which cover ~0.5 of the white-dwarf surface.

(iv) The emission lines show a broad velocity-modulated 'spin-wave' which originates in the upper accretion curtain. The spin-wave is phased with maximum blueshift at spin-flux maximum which implies that the upper pole is then pointing away from the observer. This phasing has been found in the three intermediate polars in which the phase of the spin-cycle velocity modulation has been determined. The emission-line velocities observed are lower (by a factor ~2) than would be expected using a simplistic model. A more realistic model of the accretion curtain may alleviate the discrepancy.

(v) The spin-varying components of the optical-continuum, line and X-ray emission all originate in the accretion curtain. The modulation is in all cases caused by the differing visibility of regions of the accretion curtain at different spin phases. This explains why the modulations in the different energy bands are in phase and have similar profiles. The high-velocity regions nearest the white dwarf, which produce the X-ray and optical-continuum emission, are most readily viewed when the upper pole points away from the observer – causing spin maximum. At spin minimum, these regions are obscured by the accretion curtain.

(vi) Both absorption and electron scattering contribute to modulating the X-ray emission at the spin period, effects which are naturally in phase. Modulations of the flux at both accreting poles are similarly in phase. Occultation due to the upper pole disappearing over the limb does not contribute significantly to the normal sinusoidal modulation of X-ray light curve, implying that any disappearance must be compensated for by the simultaneous appearance of the lower pole. Hence, we must see similar X-ray fluxes from both poles. If the shock height is significant then we may see both poles simultaneously at spin maximum, producing an additional modulation in phase with the accretion-curtain modulation. The 'leaky absorber' proposed by Norton & Watson (1989) is not required to model the X-ray spin modulation.

(vii) Intermediate polars differ greatly in the amplitude of the optical-continuum spin pulse. Despite this, the X-ray behaviour and the emission-line velocity behaviours are similar. The differences in the optical-continuum and line-flux spin-pulse amplitudes between intermediate polars can be explained by differences in the location of the emitting regions within the accretion curtain, coupled with differences in the system inclinations. The spin-pulse amplitudes are greatest in edge-on systems.

(viii) In order to produce the observed optical/UV beat pulse, the total luminosity in the EUV to X-ray band must be a factor of 4 greater than that seen in the 2–10 keV band alone.

ACKNOWLEDGMENTS

We thank the South African Astronomical Observatory for the allocation of telescope time for this project and we thank Fred Marang, our night assistant. We are grateful to David Buckley for a useful referee's report and to Simon Rosen for constructing Fig. 14. The *EXOSAT* data were obtained from the *EXOSAT* archive. CH is supported by an SERC Fellowship while KOM acknowledges the support of the Royal Society.

REFERENCES

Beuermann, K. & Osborne, J. P., 1988. *Astr. Astrophys.*, **189**, 128.
Buckley, D. A. H. & Tuohy, I. R., 1989. *Astrophys. J.*, **344**, 376.
Buckley, D. A. H. & Tuohy, I. R., 1990. *Astrophys. J.*, **349**, 296.

Clarke, J. T., Mason, K. O. & Bowyer, S., 1983. *Astrophys. J.*, **267,** 726.
Córdova, F. A., Mason, K. O. & Kahn, S. M., 1985. *Mon. Not. R. astr. Soc.*, **212,** 447.
Cropper, M. S., 1990. *Space Sci. Rev.*, in press.
Duerbeck, H. W., 1981. *Publs astr. Soc. Pacif.*, **93,** 165.
Hameury, J.-M., King, A. R. & Lasota, J.-P., 1986. *Mon. Not. R. astr. Soc.*, **218,** 695.
Hassall, B. J. M., Pringle, J. E., Ward, M. J., Whelan, J. A. J., Mayo, S. K., Echevarria, J., Jones, D. H. P., Wallis, R. E., Allen, D. A. & Hyland, A. R., 1981. *Mon. Not. R. astr. Soc.*, **197,** 275.
Hatchett, S., Buff, J. & McCray, R., 1976. *Astrophys. J.*, **206,** 847.
Hellier, C. & Mason, K. O., 1990. In: *Accretion-Powered Compact Binaries,* p. 185, ed. Mauche, C., Cambridge University Press.
Hellier, C., Mason, K. O. & Cropper, M. S., 1990. *Mon. Not. R. astr. Soc.*, **242,** 250.
Hellier, C., Mason, K. O., Rosen, S. R. & Córdova, F. A., 1987. *Mon. Not. R. astr. Soc.*, **228,** 463.
Hellier, C., Mason, K. O., Smale, A. P., Corbet, R. H. D., O'Donoghue, D., Barrett, P. E. & Warner, B., 1989. *Mon. Not. R. astr. Soc.*, **238,** 1107.
Hutchings, J. B. & Cote, T. J., 1986. *Publs astr. Soc. Pacif.*, **98,** 104.
Imamura, J. N. & Durisen, R. H., 1983. *Astrophys. J.*, **268,** 291.
Jablonski, F. & Busko, I. C., 1985. *Mon. Not. R. astr. Soc.*, **214,** 219.
Kaluzny, J. & Semeniuk, I., 1988. *Inf. Bull. Var. Stars,* No. 3145.
King, A. R., Frank, J. & Ritter, H., 1985. *Mon. Not. R. astr. Soc.*, **213,** 181.
King, A. R. & Shaviv, G., 1984. *Mon. Not. R. astr. Soc.*, **211,** 883.
Lubow, S. H., 1989. *Astrophys. J.*, **340,** 1064.
McHardy, I. M., Pye, J. P., Fairall, A. P. & Menzies, J. W., 1987. *Mon. Not. R. astr. Soc.*, **225,** 355.
Mason, K. O. & Rosen, S. R., 1990. In: *Accretion-powered Compact Binaries,* p. 225, ed. Mauche, C., Cambridge University Press.
Mason, K. O., Rosen, S. R. & Hellier, C., 1988. In: *The Physics of Compact Objects, Adv. in Space Res.*, p. 293, eds White, N. E. & Filipov, L. G., Pergamon Press, Oxford.
Norton, A. J. & Watson, M. G., 1989. *Mon. Not. R. astr. Soc.*, **237,** 853.
Norton, A. J., Watson, M. G. & King, A. R., 1988. *Mon. Not. R. astr. Soc.*, **231,** 783.
Norton, A. J., Watson, M. G., King, A. R., McHardy, I. M. & Lehto, H., 1990. In: *Accretion-Powered Compact Binaries,* p. 209, ed. Maude, C., Cambridge University Press.
Parmar, A. N. & White, N. E., 1988. *Memorie Soc. astr. ital.*, **59,** 147.
Patterson, J., 1984. *Astrophys. J. Suppl.*, **54,** 443.
Patterson, J. & Price, C. M., 1981. *Astrophys. J.*, **243,** L83.
Penning, W. R., 1985. *Astrophys. J.*, **289,** 300.
Pietsch, W., Pakull, M., Tjemkes, S., Voges, W., Kendziorra, E. & van Paradijs, J., 1984. In: *X-ray Astronomy '84. International Symposium on X-ray Astronomy, Bologna, Italy,* p. 67, eds Oda, M. & Giacconi, R., Institute of Space and Astronautical Science.
Pietsch, W., Voges, W., Kendziorra, E. & Pakull, M., 1987. *Astrophys. Space Sci.*, **130,** 281.
Rosen, S. R., Mason, K. O. & Córdova, F. A., 1988. *Mon. Not. R. astr. Soc.*, **231,** 549.
Siegel, N., Reinsch, K., Beuermann, K., van der Woerd, H. & Wolff, E., 1989. *Astr. Astrophys.*, **225,** 97.
Smale, A. P., Mason, K. O., White, N. E. & Gottwald, M., 1988. *Mon. Not. R. astr. Soc.*, **232,** 647.
van Amerongen, S., Kraakman, H., Damen, E., Tjemkes, S. & van Paradijs, J., 1983. *Mon. Not. R. astr. Soc.*, **215,** 45P.
Warner, B., 1985. In: *Cataclysmic Variables and Low-Mass X-Ray Binaries,* p. 269, eds Lamb, D. Q. & Patterson, J., D. Reidel, Dordrecht.
Warner, B., O'Donoghue, D. & Fairall, A. P., 1981. *Mon. Not. R. astr. Soc.*, **196,** 705.
White, N. E. & Marshall, F. E., 1981. *Astrophys. J.*, **249,** L25.
White, N. E. & Peacock, A., 1988. *Mem. S. A. It.*, **59,** 7.
Wickramasinghe, D. T., Stobie, R. S. & Bessell, M. S., 1982. *Mon. Not. R. astr. Soc.*, **200,** 605.